Powering the Future by Iron Sulfide Type Material (Fe$_x$S$_y$) Based Electrochemical Materials for Water Splitting and Energy Storage Applications: A Review

Ahmad Farhan, Wajeeha Qayyum, Urooj Fatima, Shahid Nawaz, Aldona Balčiūnaitė, Tak H. Kim, Varsha Srivastava, John Vakros, Zacharias Frontistis, and Grzegorz Boczkaj*

Water electrolysis is among the recent alternatives for generating clean fuels (hydrogen). It is an efficient way to produce pure hydrogen at a rapid pace with no unwanted by-products. Effective and cheap water-splitting electrocatalysts with enhanced activity, specificity, and stability are currently widely studied. In this regard, noble metal-free transition metal-based catalysts are of high interest. Iron sulfide (FeS) is one of the essential electrocatalysts for water splitting because of its unique structural and electrochemical features. This article discusses the significance of FeS and its nanocomposites as efficient electrocatalysts for oxygen evolution reaction (OER), hydrogen evolution reaction (HER), oxygen reduction reaction (ORR), and overall water splitting. FeS and its nanocomposites have been studied also for energy storage in the form of electrode materials in supercapacitors and lithium- (LIBs) and sodium-ion batteries (SIBs). The structural and electrochemical characteristics of FeS and its nanocomposites, as well as the synthesis processes, are discussed in this work. This discussion correlates these features with the requirements for electrocatalysts in overall water splitting and its associated reactions. As a result, this study provides a road map for researchers seeking economically viable, environmentally friendly, and efficient electrochemical materials in the fields of green energy production and storage.

1. Introduction

Hydrogen, also known as "green energy," has been generated using various technologies such as steam reforming, coal gasification, partial oxidation of methane, and water electrolysis. Hydrogen (H$_2$) has a wide range of applications, which include hydrogenation of oils and fats, ammonia synthesis (via the Haber process), methanol production, HCl generation, and so on.[1] Nowadays, H$_2$ is synthesized mainly by the steam reforming method. However, this method has certain limitations, requiring high pressure, elevated temperature, and discharging carbon dioxide into the atmosphere.[2] Finding alternative energy sources to produce H$_2$ on a large scale without harming the environment is essential for a greener society because hydrocarbons are scarce and not renewable.[3,4] Water electrolysis is vital for obtaining pure hydrogen without carbon dioxide emission into the environment,[5] especially when

A. Farhan, W. Qayyum, U. Fatima
Department of Chemistry
University of Agriculture Faisalabad
Faisalabad 38040, Pakistan
S. Nawaz, A. Balčiūnaitė
Department of Catalysis
Center for Physical Sciences and Technology
Sauletekio av. 3, Vilnius LT−10257, Lithuania
T. H. Kim
School of Environment and Science
Griffith University
170 Kessels Road, Nathan, QLD 4111, Australia

V. Srivastava
Research Unit of Sustainable Chemistry
Faculty of Technology
University of Oulu
Oulu FI−90014, Finland
J. Vakros
Department of Chemical Engineering
University of Patras
Caratheodory 1, University Campus, Patras GR 265 04, Greece
Z. Frontistis
Department of Chemical Engineering
University of Western Macedonia
Kozani GR−50132, Greece
G. Boczkaj
Department of Sanitary Engineering
Faculty of Civil and Environmental Engineering
Gdańsk University of Technology
11/12 Narutowicza Str., Gdańsk 80−233, Poland
E-mail: grzegorz.boczkaj@pg.edu.pl
G. Boczkaj
EkoTech Center
Gdańsk University of Technology
G. Narutowicza St. 11/12, Gdansk 80−233, Poland

electricity is produced from renewable sources. When hydrogen, especially green hydrogen, is employed in a fuel cell, the simple byproduct is H_2O, making H_2 a green energy source. Electrocatalytic water splitting includes hydrogen evolution reaction (HER) and oxygen evolution reaction (OER). The OER occurs at the anode, while the HER occurs at the cathode in the electrocatalytic water-splitting cell.[6,7] Since water has poor conductivity, conductive electrolytes such as 1 M KOH or 0.5 M H_2SO_4 enhance the water-splitting process.[8–10] When considering electrocatalytic water splitting, developing earth-abundant catalysts for widely producing H_2 at an affordable price is highly sought due to their availability.[11] Recent discoveries have permitted the effective exploitation of transition metals, that is, nickel, cobalt, copper, and iron, which have primarily been studied as hydroxides,[12–18] oxides,[19–22] sulfides,[18,23–25] chalcogenides,[26–28] and phosphides[29,30] for HER and OER at various pH values. Recently, many researchers have presented groundbreaking experiments using transition metal catalysts for electrocatalytic applications.[31] Transition metal sulfides are widely studied for their efficient performance in electrocatalytic water splitting. Because metal–sulfide ionic bonds are weaker than metal-oxide bonds, transition metal sulfides (TMSs) have more favorable properties for electrocatalytic performance.[32] This phenomenon improves conductance and drops the catalytic kinetic barrier for electrocatalytic water splitting. Transition metal sulfide, CuS, NiS, MnS, CoS, FeS, and CdS have been broadly researched as better-performance water-splitting catalysts during the last decade.

Among metal sulfides, iron sulfide (Fe_xS_y) and multimetallic iron sulfide-based materials have recently gained significant attention as electrocatalysts for HER, OER, oxygen reduction reaction (ORR), and overall water splitting.[33–36] Because of the high concentrations of iron and sulfur in the Earth's continental crust (3500 ppm of sulfur and 5630 ppm of iron[37]), pyrite (FeS_2) is the most prevalent inorganic material on the surface of the planet.[38]

Iron sulfide (FeS) is broadly used in supercapacitors because of its excellent electrochemical properties, low price, and abundant availability.[39] Because of its high 609 mAh g^{-1} capacity and strong electrocatalytic characteristics, FeS has sparked much interest and attention as a typical conversion-type anode material.[40] Using freeze-drying and carbonization to uniformly embed FeS nanoparticles in a carbon matrix, Xu et al.[41] significantly reduced electrode deterioration throughout the charge/discharge course and enhanced specific capacitance at 1 A g^{-1} current density. The reversible capacity (420 mAh g^{-1}) was sustained after a hundred cycles when a FeS@C/carbon cloth electrode was prepared by Wei et al.[42] using the hydrothermal method in conjunction with subsequent heat treatment. Moreover, the electrode potential of the iron–sulfur compound was higher than that of graphite electrodes,[43] along with the benefits of typical TMS electrodes.

This review paper thoroughly covers the various aspects of iron sulfide and its various composites for advanced electrochemical activities. The primary emphasis is on recent developments and breakthroughs by iron sulfide-based nanostructures in HER, OER water-splitting, ORR, and energy storage materials. We thoroughly discussed the various synthetic methods of iron sulfide and compared them to evaluate the pros and cons of various methods. Various structural forms of iron sulfide were also discussed, and it was concluded that by changing the iron sulfide structure, the overall properties of nanocomposites can be varied. Thus, more research is required to validate which structural form is better to combine with other materials (polymers, semiconductors, and carbon-based materials).

This article mainly focuses on how iron sulfide nanostructures were used to develop environmentally friendly energy and energy storage materials (supercapacitors and batteries). Various parameters (Tafel slop, stability, and overpotential) and the mechanism of the electrocatalytic process are comprehensively discussed. It was observed that iron sulfide-based nanocomposites with more synergistic effects and unique heterojunctions between them showed enhanced performance. Finally, we discussed how the efficiency and performance of iron sulfide-based nanocomposites can be improved to develop better electrochemical materials.

2. Structural Description of Iron Sulfide

Mackinawite (FeS), pyrite (FeS_2), greigite (Fe_3S_4), pyrrhotite ($Fe_{(1-x)}S_{(x=0-0.2)}$), and marcasite (FeS_2) are the most common iron sulfide in solid phases (**Figure 1**). Therefore, the amount of iron inside affects a biomaterial's phase, form, and physical and chemical characteristics. Each iron atom in FeS is usually coordinated with four sulfur atoms, giving the compound a tetragonal structure. The monoclinic hexagonal structure is seen in $Fe_{1x}S$. Stable iron (II) disulfides with cubic structures can be formed when FeS_{2p} is present. When comparing FeS_{2m} to FeS_{2p}, it will be noticed that the former is an orthorhombic metastable iron (II) disulfide while the latter is a cubic metastable iron (II) Fe (III) sulfide. The hexagonal Fe_9S_{11} is associated with the $Fe_{1-x}S$ phase.[38]

Iron atoms in FeS are coordinated with four sulfur atoms at equal distances using tetrahedral bonds, giving the compound a layered tetragonal structure. Coordinated with four equally spaced sulfur atoms is a single iron atom. In metric terms, the Fe–Fe separation is 2.5967 Å. Also, Fe–Fe bonding plays a significant role in FeS. Sheets containing Fe are stacked along the *C*-axis to evaluate the consequences of van der Waals forces caused by the S atoms. There is a 5Å separation between each of these levels. Fe_2S_2 has a very similar structure to that of FeS. As with NaCl, the S_2 ion is centrally placed in a cube in FeS_2, but this time it's a tetrahedron. The symmetry of the cubic structure is somewhat poor.

The inverse spinel structure of Fe_3S_4 consists of eight Fe atoms in the tetrahedral A-sites and sixteen Fe atoms in the octahedral B-sites. Fe_3S_4 has a unit cell size of 9.876 Å. In Fe_3S_4, the cubic structure generates a tightly packed array of S molecules connected by smaller Fe units. A hexagonal supercell for Fe_7S_8 has been proven.[44,45] Fe_9S_{10} was found to have a structure characterized by the optimal vacancy site distribution for the NiAs base structure.[46]

3. Synthetic Methods of Iron Sulfide Formation

Iron sulfide at the nanoscale includes several different iron and sulfur compounds. Many synthetic iron sulfide methods are discussed in detail (**Figure 2**). Moreover, the most widely reported
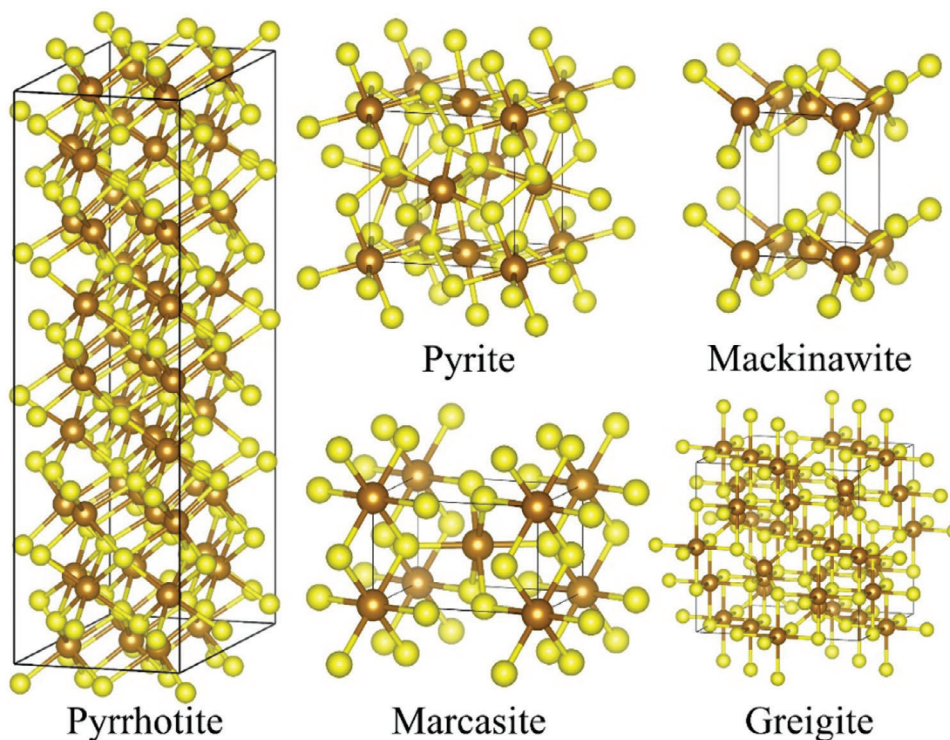
ADVANCED
SCIENCE NEWS

www.advancedsciencenews.com

NANO · MICRO

small

www.small-journal.com

Figure 1. Various structural forms of iron sulfide

synthetic techniques for producing iron sulfide phases are discussed in **Table 1**.

3.1. Hydrothermal Synthesis

The utmost prevalent hydrothermal process for producing iron sulfide is thermal degradation. Dissolving $FeCl_3 \bullet 6H_2O$ in water is the first step in the hydrothermal synthesis of nFeS. After adding the NaOAc and organosulfur compounds, that is, diallyl sulfide, allyl methyl sulfide, diallyl disulfide, cysteine, diallyl trisulfide, cystine, methionine, or glutathione (GSH), the as-prepared solution was mixed under vigorous stirring. Next, it was sonicated for 10 min before being placed in a stainless steel autoclave coated with Teflon. The reaction occurs in 12 h at 200 °C followed by washing residues. The items were dried at 60 °C for 3 h.[62]

Aqueous Fe(III) diethyl dithiophosphate is produced by reacting $(C_2H_5O)_2P(S)NH_4$ and $FeCl_3$ with surfactant hexadecyltrimethylammonium bromide and then reacting with the only precursor, $[(C_2H_5O)_2P(S)S]_3FeS_2$.[63] Ethanolamine and thiourea were mixed in a solution of $FeCl_3 \bullet 6H_2O$ dissolved in ultrapure water to fabricate FeS. The liquid was stirred for 25 min before being placed in a Teflon-lined autoclave for a 12-h reaction at 180 °C. Fe_3S_4 is synthesized in a way that is distinct from FeS. Polyvinyl pyrrolidone (PVP) was added to a mixture of thiourea, ethylene glycol, $FeCl_3 \bullet 6H_2O$, and hydrogen peroxide and then heated to 180 °C for 18 h to prevent the NPs from becoming too large or clumping together.[64] $Fe_{1-x}S$ single crystals were formed hydrothermally by reacting $K_{0.8}Fe_{1.6}S_2$, iron powder, thiourea, and NaOH in deionized water at 120 °C for 3–4 days.[65] Zheng and coworkers stated that while altering the structure of Fe_3S_4, ionic liquids that form extended hydrogen bond systems were employed to build higher structures based on the hydrothermal approach. The hydrothermal method yields a product with
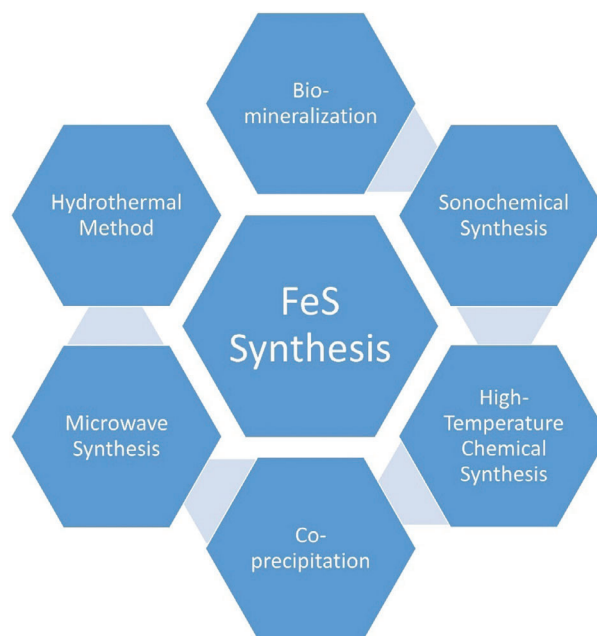

Figure 2. Various synthetic methods to prepare iron sulfide.

Table 1. Lattice spaces, appearances, and sizes of various iron sulfides.

Phases	Synthesis method	Morphology	Size thickness [nm]	Lattice space [nm]	Application	Refs.
FeS	High-temperature chemical synthesis	Nanoplates	32–36	0.286	Antimicrobial	[47]
	Sonochemical synthesis	Spherical	6–20			[48]
	Hydrothermal synthesis	Flower-like	3000		Supercapacitors	[49]
	Biomineralization	Spherical	2–7		Antimicrobial	[50]
FeS$_2$	High-temperature chemical synthesis	Cubic	60–200		–	[51]
	Microwave	Big particles	200		Coal pyrolysis	[52]
	Hydrothermal synthesis	Uniform nanowires	40–60	0.269	–	[53]
	Thermal decomposition	Nanoribbons	100–250	0.313	ORR	[54]
	Biomineralization	Nanodots	7		Biomedical	[55]
	Low-temperature synthesis	Hexagonal	600–700		Hg (II) removal	[56]
Fe$_2$S$_4$	Hydrothermal synthesis	Plates	2000-–5000 17.7	0.298	Biomedical	[55]
	Hydrothermal synthesis	Nanocrystals	2.5–4.5		Biomedical	[55]
	Hydrothermal synthesis	Hexagonal nanoplates	(side length) 100		Corrosion	[57]
	Co-precipitation	Irregular particles	50–100	0.572	–	[58]
Fe$_7$S$_8$	Hydrothermal synthesis	Spherical	5.6		Lithium-ion battery	[59]
	Solvothermal synthesis	Hedgehog-like	10 000		Lithium-ion battery	[60]
	Flux	Nanorods	200 1500–2000 (length)		Biomedical	[55]
	Hydrothermal synthesis	Nanowires		0.289	Catalytic activity	[61]

improved controllability and dispersibility; however, iron oxide contamination may affect the synthesis of iron sulfide. Meanwhile, X-ray diffraction patterns for hydrothermally generated materials suggest that multiphase iron sulfide formation is simple by this method.[66]

3.2. Microwave Synthesis

Compared to traditional heating techniques, the main benefits of microwave-assisted procedures include a shorter reaction time, a narrower particle size distribution, and greater purity.[67] Because of its intense dipole moment, ethylene glycol is an ideal microwave solvent. Atmospheric nitrogen is used in a microwave reaction with PVP–K-30, FeSO$_4$.7H$_2$O, and S powder in ethylene glycol to produce FeS$_2$ microspherolites.[68] It is essential to highlight that this new method does not seem to enhance the aggregation phenomena, although it may be preferable.

3.3. Precipitation

This process is carried out at mild temperatures and allows the formation of mostly Fe$_3$S$_4$. It includes dissolving iron (II) sulfate heptahydrate and sodium sulfide in ultrapure distilled water. Drop by drop, the solution was mixed with the acetic acid while stirring for several minutes to get the pH down to 3.0. A nitrogen environment was used in the reaction in order to maintain an inert environment.[69] In a continuous stirred tank reactor, eco-friendly synthesis was accomplished. According to earlier reports, co-precipitation necessitates more rigorous synthesis con-ditions than other procedures, and the resulting compounds may exhibit poor homogeneity.[70]

3.4. High-Temperature Chemical Synthesis

The chemical production of FeS$_2$ has been described, and it involves high temperatures. The degassed mixture of oleylamine (OLA), trioctylphosphine oxide (TOPO), and iron (II) acetylacetonate (Fe(acac)$_2$) was heated at 110 °C for 1 h.[71] Subsequently, the mixture was quickly heated to 220 °C for 1 h while being vigorously magnetically stirred in an atmosphere of nitrogen. The solution was then heated at 220 °C for 1 h before introducing the sulfur. After the solution had cooled, the FeS$_2$ nanoplates were developed by adding ethanol. It has also been claimed that Fe$_{1-x}$S and Fe$_3$S$_4$ can be synthesized by using a high-temperature synthesis method.[72]

3.5. Sonochemical Synthesis

The production of nanoparticles is achieved by applying high–frequency ultrasound radiation (ranging from 20 kHz to 10 MHz) on molecules in the sonochemical synthesis process.[73] First, a solution of sodium sulfide in distilled water was synthesized. Subsequently, FeSO$_4$•7H$_2$O was liquefied in a mixture of polyethylene glycol and double distilled water (1:1). After continually sonicating the solution mentioned above for 30 min, a drop of the sodium sulfide solution containing the Triton-X surfactant was added. Then PVP was added, the system was mixed with ultrasound for 30 min, and iron sulfide nanoparticles were obtained.[48]

3.6. Other Chemical Methods

There have been reports of specific peculiar synthetic chemical techniques. Nanoparticles of FeS_2 were first reported as being synthesized at low temperatures in 2022.[74] In a nutshell, in an anaerobic pH 5.6 acetate buffer, sodium polysulfide (Na_2S_x) and $FeCl_3$ were blended. After that, the black mixture was reacted in an oil bath at 90–100 °C for 4 h to generate a grey FeS_2 substance. Then, 1D Fe_7S_8 was synthesized using flux techniques. The reaction occurred in a furnace between 750 and 850 °C.[55]

3.7. Biomineralization

Iron sulfide biosynthesized by microorganisms is more effective for therapeutic uses.[44] In the presence of certain enzymes, FeS nanoparticles (NPs) are formed within microorganism cells after interacting with target ions.[75] As a bonus to green production, biological processes make iron sulfide more biocompatible because they are stable over a pH range (1–12).[76] Research has shown that bacteria can create FeS_2, Fe_3S_4, and FeS NPs. A magnetotactic bacteria can biomineralize Fe_3S_4 and FeS_2.[77] Sulfate-reducing bacteria cultured on iron-containing substrates created FeS particles.[78] Using magnetotactic bacteria, Bazylinski and colleagues reported the production of Fe_3S_4.[79] Charnock and coworkers showed that sulfate-reducing bacteria might create $Fe_{1-x}S$.[80] The microbes then generated FeS NPs at the surface, demonstrating that the spongy structure of the iron sulfide NPs was insufficient to impede the metabolic processes. These tests confirmed the validity of using this technique for effective NP manufacturing. FeS Quantum dots (QDs) and FeS_2 have been synthesized using chemical biomineralization techniques.[72,81,82]

4. Parameters of Water Splitting

Hydrogen may be produced by electrochemically converting water to hydrogen and oxygen, requiring free energy of 238 kJ mol^{-1} (Equation (1)).

$$2H_2O_{(l)} \rightarrow 2H_{2(g)} + O_{2(g)} \tag{1}$$

Water splitting may look like a simple reaction since it is an extension of standard electrochemistry, but it requires substantial effort because of energy loss embedded in mechanical complexity.[83,84] The water-splitting process entails two distinct halves: The reaction involves the release of hydrogen gas at the cathode and the oxygen gas is generated at the anode.[85,86]

There are several possible routes for oxygen evolution, including metal oxide, oxy-hydroxide, and hydroxide, and it is not yet known which one is used. In 3D transition metals, movement is proportional to the electron density of the e_g and t_{2g} orbitals. As a result of the intercalation of hydroxyl radical (•OH) and the cleavage of O_2 at the surface, total OER activity is changed.[87] The electron density of the electrode should be high for optimal −OH group binding and subsequent O_2 cleavage. Considering these factors, the electronic configuration of Fe group metals (Fe, Ni, and Co) is favorable for OER. In the case of iron, the large electron density effectively slows down the $^-$OH interaction, even though repulsion is encouraged. Therefore, the hydroxide/oxide phase generated in OER behaves as the proper surface of the catalyst. In contrast, architecture in the structures of catalysts made up of transition metals is activated with various combinations.

Because the steps in HER are centered on the H_2 desorption and adsorption processes, the mechanism is more straightforward than in OER. The first step in the hydrogen evolution reaction, also known as the Volmer step, is hydrogen adsorption, and the subsequent steps are hydrogen desorption from the electrode surface, known as the Volmer–Tafel step or Volmer–Heyrovsky step, respectively.[36] Depending on the amount of exposed active surface area, desorption at the working electrode can be either chemical or electrochemical. For example, platinum follows the Tafel process for hydrogen adsorption and desorption with optimum free energy and a high exposed surface area on top of the 'volcano plot.' OER and HER have quite different reaction mechanisms depending on the electrolytes utilized. In an acid, hydrogen ions combine with electrons to release hydrogen and water to release oxygen. The electrode surface in alkali reacts with OH ions for OER and H_2O for HER. Because of this, OER is excessively rapid and HER too slow in alkaline environments, and vice versa in acidic ones. The equation is as follows Equations (2–5).

In acidic media,
cathodic reaction

$$4e^- + 4H^+ \rightarrow 2H_2 \tag{2}$$

anodic reaction

$$2H_2O \rightarrow 4H^+ + 4e^- + O_2 \tag{3}$$

In alkaline media,
cathodic reaction

$$4e^- + 4H_2O \rightarrow 4OH^- + 2H_2 \tag{4}$$

anodic reaction

$$4OH^- \rightarrow 2H_2O + 4e^- + O_2 \tag{5}$$

Since high rate activity for HER and OER demonstrated transition metal-based catalysts in essential circumstances, It is evident that the creation of realistic amounts of H_2 using earth-abundant minerals is beyond the capabilities of bifunctional catalysts.[36,88,89] However, the acid's corrosive properties reduce the catalysts' durability. The goal is to reduce the prevalence of overpotentials so that water can be divided at a large enough scale using less anodic and cathodic energy inputs while maintaining a durable electrode.

4.1. Tafel Slope

Tafel slope values are used as a measure of the intrinsic electron transport at the electrode/electrolyte contact. For larger anodic and cathodic overpotentials, the Butler–Volmer equation that was obtained from quantum mechanical principles was found to be in good agreement by the use of the Tafel equation, thereby (j) is the density of current being proportional to the (i_0) density of

ADVANCED
SCIENCE NEWS
www.advancedsciencenews.com

NANO · MICRO
small
www.small-journal.com

exchange current and the Tafel curve (*b*) being inversely proportional to (*j*). It can find written as in Equation (6).

$$i = i_0 \log(\eta/b) \tag{6}$$

where *i* is the current density, i_0 is the density of exchange current, *η is the* overpotential, and *b* is the Tafel constant. The polarization curves are commonly employed to extract Tafel slopes; the log of current density is obtained against the overpotential, and the analyzed results reveal the Tafel curve values in mV dec^{-1}. In this case, however, because of potentiodynamic, the current detected is not necessarily the true current, and there is a chance of inconsistency, which will cause the Tafel slope values to vary. Therefore, the steady-state current can be obtained with more precision using potentiostatic analysis, and the static current densities witnessed at various overpotentials can be used to get the values of the Tafel slope. In addition to comparing overpotentials, the kinetics of multiple electrodes can be acquired from the obtained Tafel slope values. Different catalysts exhibit varying degrees of activity at different overpotentials and current densities.[36] OER is estimated to be around 30 mV dec^{-1} if four electron transfers occur at the contact, though this estimate can shift with variations in kinetic efficiency.[88] Like the hydrogen evolution reactions, the Tafel slope measurements show that the electrode uses electrochemical or chemical desorption. For Pt-based catalysts, if the value is close to 30 mV dec^{-1}, the reaction progresses through the Tafel mechanism and is accompanied by chemical desorption. Therefore, from Tafel slope values, the charge transfer kinetics can be determined; potentiostatic analysis should be used to get the log current densities so that the correct Tafel curve values can be observed and related to the kinetics of the working electrodes in the preferred HER or OER study.[89]

4.2. Overpotential

Among the available options, electrocatalytic water splitting is the most practical. Due to its stable octet structure, water is thermally non-spontaneous, having a net free energy change of +237 kJ mol^{-1}.[87] H$_2$ evolution had a standard reduction potential of zero V versus RHE (reversible hydrogen electrode). In contrast, O$_2$ evolution has a potential of 1.23 V. Therefore, the theoretical potential required for water splitting is 1.23 V Equation (7).

$$H_2O \rightarrow H_2 + 1/2O_2 \quad E^o = 1.23V \ vs \ RHE \tag{7}$$
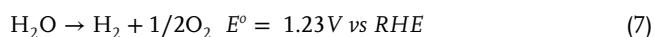
Nevertheless, the surplus potentials, also known as overpotentials, are dragged by the aforementioned aided resistances, which include the electrode, circuit, distance, and kinetic processes involved in both HER and OER. The mechanism of OER is more complicated than HER as it includes a four-proton linked electron transfer reaction, and every step in the process carries additional overpotentials. Quantitative measures for assessing the performance of novel catalysts are the overpotentials at a given current density (e.g. 300, 250, 100, and 100 mA cm^{-2}).[90] For an electrocatalyst to show good electrochemical activity, its overpotential must be low. Lower overpotential means higher perfor-

mance and vice versa.[91] Doping can lower overpotential, creating synergistic heterojunctions between materials, oxygen vacancies, and so on.[92] The linear sweep voltammetry (LSV) plot may be used to calculate overpotential. The overpotential for OER is the voltage at a current density of 10 mA cm^{-2} minus 1.23 V (theoretical voltage for EWS); for HER is the voltage at a current density of 10 mA cm^{-2}.[93]

4.3. Stability

For electrocatalytic water splitting, a catalyst's durability is essential over the long term to discuss its applicability in practice. This can be verified by the potentiodynamics study, that is, cyclic voltammeter scan rates are in the range of 1000–5000 cycles, and potentiostatic analysis, that is, chronoamperometry. The stability of the catalysts is ensured by the fact that there is almost no change in activity before and after the stability investigations. To evaluate the strength of a catalyst in potentiodynamic conditions, one looks at how much the overpotential shifts for a given current density. The destructive nature of the acid and the anodic overpotentials both damage the electrode surface substantially, making stability in acidic circumstances the bottleneck for OER. Electrodeposition and hydrothermal methods that mimic the growth of Ni and Cu foams produce materials with excellent stability. The electrode material adheres tenaciously to the pores of the conducting materials, which is one of the most important aspects of stability. Recent research has demonstrated the strength of catalysts based on 3D transition metals in basic HER and OER.[87] Bifunctional catalysts are being developed to replace rare metals in applications demanding high stability and activity. Better catalysts for electrocatalytic water splitting in a vast range of pH circumstances cannot be derived without carefully analyzing and considering several factors, including overpotential, TOF, Tafel slope, and stability.

5. OER

Nowadays, there is a growing awareness of the hazards to human life caused by changing energy consumption and a deteriorating environment.[94,95] As a result, improving viable energy storage and transformation devices for the future, that is, metal–air batteries, fuel cells, and water-splitting technologies, has become vital.[96–98] The electrocatalytic OER and ORR are the basic electrochemical processes of the aforementioned viable devices.[99–101] However, their low reaction rate and poor chemical stability limit their broad utilization.[96,102,103] The ORR and OER's highly active electrocatalysts have been novel metal composites, that is, Ru/Ir- and platinum-based.[104,105] These two electrocatalysts are expensive and have limited reserves, limiting their large-scale manufacture.[106,107]

Many reaction pathways for OER on heterogeneous electrocatalysis have been postulated centered on kinetic studies[108–110] or theoretical density functional theory (DFT) calculations.[111,112] Nevertheless, no experimentally confirmed reaction mechanism for heterogeneous catalysts has yet been presented. Bockris created pioneering kinetic models for several OER processes. Bockris revealed that a rate-determining step (rds) inside a reaction
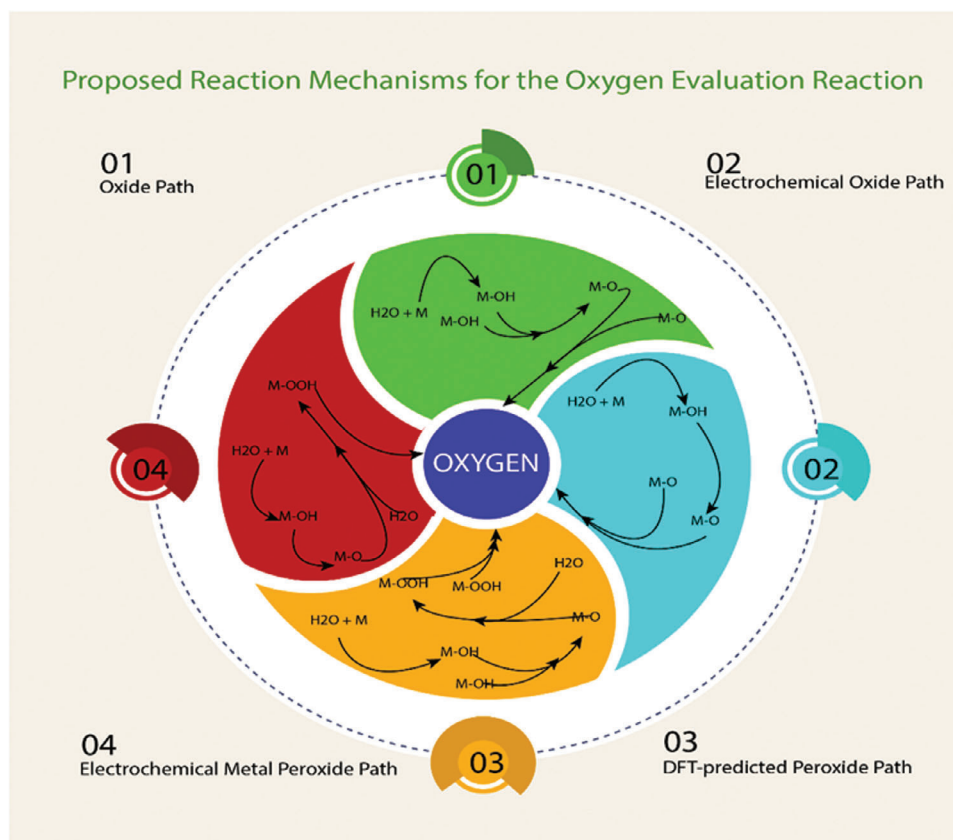
ADVANCED
SCIENCE NEWS
www.advancedsciencenews.com

NANO · MICRO
small
www.small-journal.com

Figure 3. Four types of OER mechanisms, including oxide path, electrochemical oxide path, electrochemical metal peroxide path, and DFT-predicted peroxide path

mechanism governs the Tafel slope. This study assumed that the rate-determining step rds are one step in each process mechanism and that only the rate-determining step reactant may make up a significant surface coverage.[108] To compare the electrochemical oxide route to RuO$_2$, the Tafel slope analysis indicated an extra chemical re-arrangement step of the M–OH species between reactions, as shown in **Figure 3**. Four basic mechanisms proposed are i) the DFT-predicted pathway, ii) the electrochemical metal peroxide pathway, iii) the electrochemical oxide pathway, and iv) the oxide pathway.

5.1. Iron Sulfide-Based Nanocomposites for OER

Zhang et al. reported that due to their exceptional activity in the OER, transition metal sulfide electrocatalysts have garnered a lot of interest. Here, hydrothermal and vulcanization techniques were used to synthesize the highly effective iron-doped nickel sulfide catalyst effectively based on functionalized N-doped reduction graphene oxide (Fe–NiS/NrGO). The doped Fe alters the electronic structure of NiS, speeding up the kinetics of OER. The homogeneous dispersion of Fe–NiS nanoparticles is facilitated by the NrGO, which has a large specific surface area and high conductivity. This increases the active catalytic area and speeds up the charge transfer rate. The Fe–NiS(2)/NrGO has exceptional OER performance, achieving a current density of 100 mA cm^{-2}

in 1.0 M KOH with an overpotential of 344 mV, and a Tafel slope as low as 47 mV dec^{-1}. Compared to commercial RuO$_2$, Fe–NiS(2)/NrGO exhibits superior OER performance.[113]

Wang et al. reported that the optimization of electrocatalyst activity is achieved by revealing the actual catalytic active species by surface reconfiguration of the catalysts during the OER. This article presents a straightforward method for achieving Fe$_{1-x}$ S nanocrystals/ultra-thin carbon (Fe$_{1-x}$ S NCs/@ UT–C) nanolamellar structure electrochemical reconfiguration in its entirety during the oxygen evolution reaction (OER) process. The quick and thorough reconfiguration is facilitated by the homogeneous dispersion of Fe$_{1-x}$ S nanocrystals on the very thin carbon layer. Fe$_{1-x}$ S is quickly reconfigured to produce new catalytically active amorphous iron-based oxide species, combined with an incredibly thin carbon layer to promote OER charge transfer. In addition to allowing for the reduction of ohmic losses, more thorough graphitization of the ultra-thin carbon layer also improves the material's overall electrical conductivity and OER activity. With a Tafel slope of 55 mV dec^{-1} and a low overpotential of just 303 mV at 100 mA cm^{-2}, the Fe$_{1-x}$ S NCs/@UT–C precatalyst exhibits significant OER activity. Furthermore, in alkaline circumstances, the redesigned catalyst exhibits high stability for 168 h.[114]

Deng et al. reported that promoting the electrochemical synthesis of oxygen from water requires the development of effective non-noble metal catalysts. This study shows that a
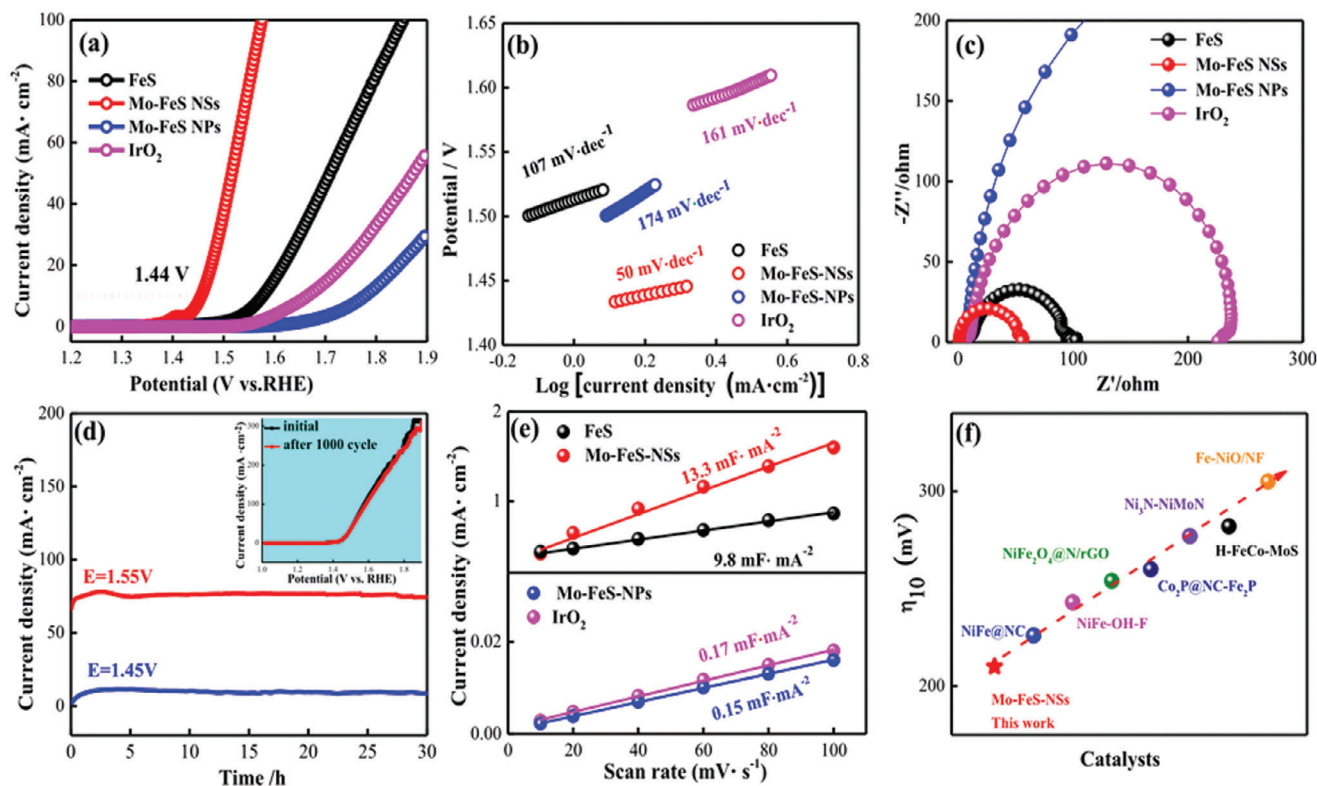
ADVANCED
SCIENCE NEWS
www.advancedsciencenews.com

NANO · MICRO
small
www.small-journal.com

Figure 4. a) Polarization curves of OER, b) Tafel slopes for several catalysts, c) EIS spectra, d) MoFeS NSs current against time curves at 1.45 and 1.55 V versus RHE, as well as LSV current versus time curves before and after a 1000 cycles (inset), e) double-layer capacitance, and f) evaluating the overpotential of OER versus the most recent reports. Reproduced with permission from.[97] Copyright 2020, Elsevier.

straightforward sulfurization technique may be used to create a FeS/Co_3S_4 heterostructure composite on carbon cloth that resembles a flower. Better than the FeS and Co_3S_4 electrodes, the as-prepared FeS/Co_3S_4 composite exhibits good OER performance with a modest Tafel slope of 58 mV dec^{-1}, and a low overpotential of 252 mV at 10 mA cm^{-2}. Furthermore, the FeS/Co3S4 composite exhibits exceptional structural stability with no deterioration throughout extended testing. The enhanced specific surface area and heterojunction formation of FeS/Co_3S_4 are responsible for the enhanced OER catalytic performance of the FeS/Co_3S_4 composite. Furthermore, according to theoretical calculation findings, the FeS/Co_3S_4 heterojunction exhibits a greater adsorption capacity to •OH, which is more advantageous for the OER than the single FeS and Co_3S_4 counterpart.[115]

The electrocatalytic performance might be improved by incorporating anion flaws and amorphous structures into the ultrathin 2D structure of iron sulfide. A simple method for manufacturing ultrathin, amorphous Mo–FeS nanosheets (NSs) were prepared and rich in sulfur defects. Mo–FeS nanosheets showed an overpotential of 210 mV at 10 mA cm^{-2}, the Tafel slope of 50 mV dec^{-1}, and the maintenance of such worthy catalytic stability above 30 h all showed that the Mo–FeS NSs benefit from their ultra-thin, amorphous nanomaterial and the synergy effect of molybdenum doping and sulfur imperfection, resulting in their exceptional electrocatalytic activity toward OER in basic medium (**Figure 4**a–f). Mo–FeS NSs outperformed IrO_2, and other testified top-performing electrocat-

alysts regarding catalytic efficiency. In addition to helping the OER kinetics, sulfur vacancies boost the activity of nearby iron-active sites.[97] A co-precipitation technique and subsequent pyrolysis in an N_2 environment were used to prepare a series of NiSFeS/N, sulfur co-doped carbon for use in an OER. In Ni_xFe_yS/NSC, the NiSFeS hybrid was consistently incorporated with S, N co-doped carbon. Exhibiting strong OER catalytic activity, Ni_xFe_yS/NSC was adjusted to provide a Tafel slope of 30.9 mV dec^{-1} in 1 M KOH and an OER overpotential of 239 mV, resulting in a 10 mA cm^{-2} current density. The OER catalytic activity of these compounds was superior to that of IrO_2 but also on par with that of the most recently reported NiFe-based sulfides for OER. Research showed that the hybridization of NiS and FeS enhanced OER. The catalytic performance was improved due to the increased number of sulfides as active species due to the hybridization process. Hybridization also increased the amount of graphitic and S, nitrogen co-doped carbon, which enhanced charge transfer efficiency and produced petal-like morphologies, contributing significantly to a larger ECSA.[116] Various iron sulfide-based nanomaterials have been studied (**Table 2**). Mo–FeS nanosheets and NiSFeS/N, S co-doped carbon showed overpotential 210 and 239 mV, respectively. Mo–FeS nanosheets showed better performances due to enhanced charge transfer among the heterostructure. The unique heterostructure between Mo and Fe was responsible for enhanced oxygen evolution performance compared to other nanocomposites.

6. ORR

ORR has gained significant research interest in electrochemical catalysis for renewable and clean energy technologies, that is, fuel cells and metal–air batteries.[126] Given the cost and storage constraints, significant effort has been expended in creating novel, inexpensive catalysts with large stability and activity to replace costly platinum-based catalysts. Many non-platinum-based electrocatalysts containing transition metal phosphides,[127,128] oxides,[129,130] sulfides,[131–137] or nitrides[138,139] have been extensively examined. Due to their comparatively high conductance and activity, TMSs drew the most interest. Aside from component regulation, various additional characteristics, that is, accessible active sites, electrode geometrical structure, and electrical conductivity, were revealed to have a significant impact on catalytic activity.[140] ORR mainly comprises two mechanisms, *viz.* associative and dissociative responses, as shown in **Figure 5**.

6.1. Iron Sulfide-Based Nanocomposites for ORR

To manufacture clean and sustainable fuel via electrochemical methods, it is essential to fabricate highly efficient, inexpensive, and earth-abundant electrocatalysts for the oxygen reduction reaction. Iron sulfide/graphene hybrid was synthesized using a simple hydrothermal approach in an oxygen reduction reaction. Catalyst morphology showed that iron sulfide NPs are uniformly covered on the surface of reduced graphene oxide sheets. The hybrid's half-wave potential is +0.845 V, its onset potential is +1.0 V (against a reversible hydrogen electrode), and its oxygen reduction catalytic efficiency is greatly enhanced (**Figure 6a–d**). It also shows remarkable long-term stability in alkaline environments. The hybrid electrode was more stable and resistant to methanol than the reference platinum/carbon electrode under basic conditions. Exceptional activities were observed due to the synergistic linkage between FeS and graphene. Based on the findings, metal sulfide could be a viable alternative to platinum as a catalyst for the ORR.[141] Before the oxidative polymerization process begins, the precursor is made by synchronizing SCN^- with Fe^{3+} ions adsorbed in situ within the polypyrrole matrices ($PPy–Fe^{3+}$). The $FeN_x/S–NC$ catalyst, including $Fe–N_x$ active sites and thiophene-like sulfur structures, was obtained by further pyrolyzing the $PPy–Fe^{3+}–SCN^-$ precursor. In addition, the specific
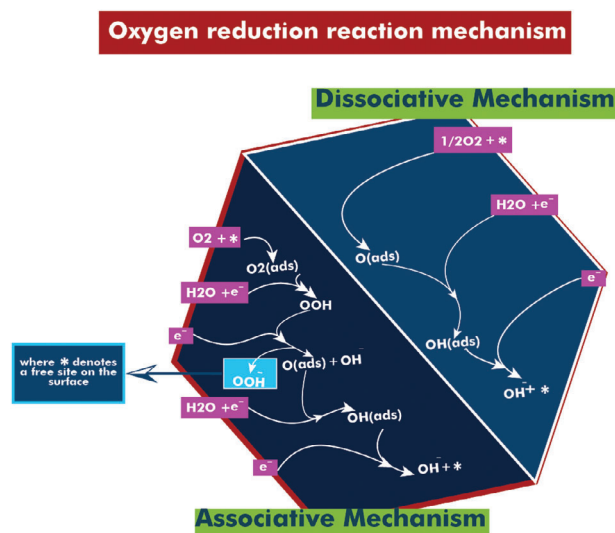

Figure 5. Associative and dissociative mechanisms of an oxygen reduction reaction mechanism.

Table 2. Comparison of various FeS-based nanocomposites for effective OER.

Composite	Tafel slope [mV dec⁻¹]	Overpotential [mV]	Current density [mA cm⁻²]	Double layer capacitance [mF cm⁻²]	Resistance [Ω]	Stability [h]	Synthesis method	Refs.
NiFeS@NF	34.8	243	10	4.38	9.5	12	One-step electrodeposition strategy	[117]
Co_9S_8–CuS–FeS	79	300	10	1.51	26	10	Hydrothermal method	[118]
Co–Fe–S/N-doped carbon composites	50	340	10.5	–	–	7	Calcination route	[119]
Co–Fe–S nanocomposite	92.7	283	10	40.6	10.1	50	Solvothermal route	[120]
FeS/Fe_2O_3/IF	51.17	266.5	10	3.35	9.57	50	Solvothermal method	[121]
FeS/FeO_xH@Fe nanosheets	71	245	10	2.23	–	36	One-step co-deposition method	[122]
Mo–FeS NSs	50	210	10	13.3	–	30	Facile hydrothermal strategy	[97]
NiS–FeS/NSC	≈30.9	≈239	10	3.105	10.37	8.3	Simple co-precipitation method	[116]
FeS_2 CL@WS_2	54	260	10	26.32	2.3	5	Solvothermal method	[123]
$CoFe/Co_8FeS_8$/CNT	38	290	10	22.22	16.7	18	Microwave-assisted sulfidation and annealing process	[124]
$FeNi(OH)_x$/FeS/IF	63	273	100	–	–	12	Ultrafast surface modification process	[125]
NiFeS@NF	34.8	243	10	4.38	9.5	12 h	One-step electrodeposition strategy	[117]

**ADVANCED
SCIENCE NEWS**

www.advancedsciencenews.com

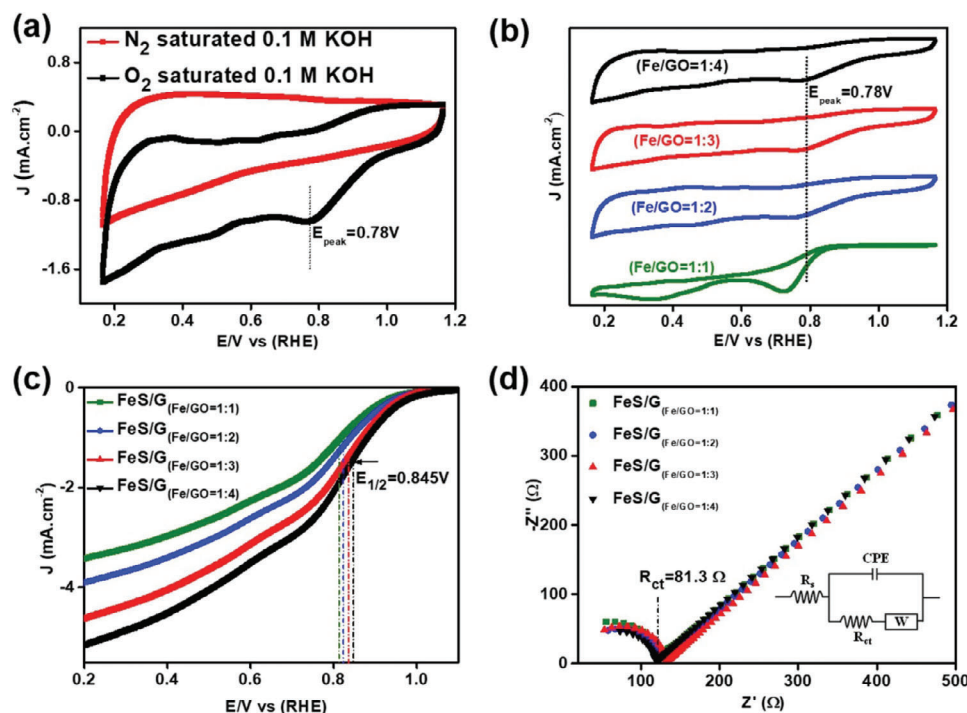NANO · MICRO

small

www.small-journal.com

Figure 6. a) CV curves of the FeS/G hybrid in O^{2-} and N^{2-} saturated 0.1 M KOH electrolyte; b) comparison of ORR activity of different FeS/G; c) LSV of different FeS/G hybrids; d) EIS outcomes of altered FeS/G hybrids in 0.1 M potassium hydroxide electrolyte in the frequency range of 10^5-10^{-2}. Reprinted with permission.[141] Copyright 2019, American Chemical Society.

surface area of the $FeN_x/S-NC$ catalyst is higher than that of the FeN_x-NC catalyst without SCN^- in the precursor.

The valence band of $FeN_x/S-NC$ is higher (at -7.27 eV) than FeN_x-NC (at -7.76 eV), resulting in a lower energy gap with the LUMO oxygen level. The ORR catalyst based on $FeN_x/S-NC$ had one of the most extraordinary catalytic activities centered on Fe–N–C reported, with an initial potential of 1.02 V and a half-wave potential of 0.90 V in an alkaline environment. After 5.5 h, the $FeN_x/S-NC$ catalyst still upholds 91% of its initial current density, making it more stable than Pt/C. Furthermore, when used as the cathode material for a Zn–air battery, $FeN_x/S-NC$ demonstrates higher peak power and specific capacity than Pt/C.[142] Iron sulfide/graphene nanomaterial and $FeN_x/S-NC$ showed better ORR activity than other iron sulfide-based composites (**Table 3**). Iron sulfide/graphene showed the best ORR ac-

tivity with an onset potential of 0.845 mV and electron transfer number 4. Heterojunction between graphene and iron sulfide resulted in a decrease in charge resistance and an increase in onset potentials.

7. HER

Probably, HER has been the most investigated reaction in electrocatalysis ever since the scientific breakthrough in 1789.[147] This process contains two straight protons–electron transfers while a side reaction does not occur.[148] Many studies focused on understanding how different physical features of metals, including their surface morphology, impact HER kinetics.[149] This extensive investigation helped clarify active sites' chemistry and their relationship to HER activity. Among other

Table 3. Comparison of various FeS-based nanocomposites for effective ORR.

Composite	Onset potential	Electrolyte	Electron transfer	Resistance [ct]	Stability	Stability efficiency	Synthetic method	Refs.
$FeN_x/S-NC$	1.02 V	6 M KOH	4.0	–	5.5 h	91%	Double-doping strategy	[142]
FeS/G	0.845 V	0.1 M KOH	4.0	102.5 Ω	5.5 h	94.3%	Hydrothermal method	[141]
FeS/ZnS@N,S–C-900	1.0 V	0.1 M KOH	4.0	–	5.5 h	90%	One-step pyrolysis	[143]
FeS_2@rGO composite	–	0.1 M KOH	4.0	–	1.3 h	94.3%	A facile method	[144]
FeN_x/FeS_x– CS–CNT composite	0.94 V	0.5M H_2SO_4 or 0.1M KOH	4.0	0.055 Ω at 0.40 V	12 h	–	Pyrolysis process	[145]
Fe_3C/FeS encapsulated carbon with a heteroatom	0.91 V	0.1 M KOH electrolyte	3.99	–	–	87%	Pyrolysis process	[146]

**ADVANCED
SCIENCE NEWS**

www.advancedsciencenews.com
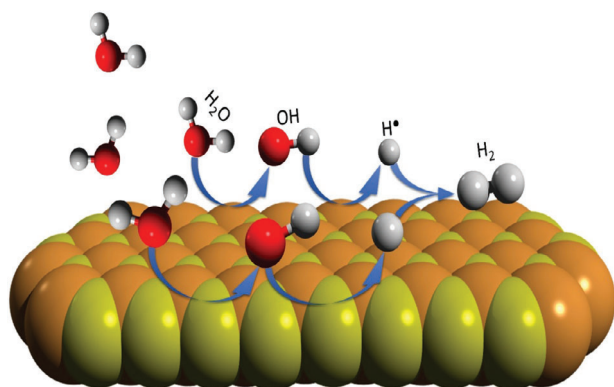
**NANO · MICRO
small**

www.small-journal.com

Figure 7. Mechanism of hydrogen evolution reaction of iron sulfide (Fe: Brown spheres, S: Yellow spheres)

factors, HER activity is significantly affected by acidic or alkaline mediums.[150]

Nobel metals like platinum and platinum–based substances are highly effective but costly and less available electrocatalysts for hydrogen/oxygen energy sources.[48] Due to these constraints, researchers sought low-cost, available materials that may replace these expensive metals as capable catalysts for diverse possible sources, hydrogen production, and energy-related applications.[151,152] Recent initiatives have replaced noble metals with transition metal complexes, that is, nickel, tungsten, cobalt, and molybdenum.[153] Metal sulfides, that is, FeS, CoS_2, ZnS, and Bi_2S_3, have been effectively utilized for supercapacitors, lithium-ion batteries, and HER.[154]

Among all metal sulfides, FeS has remarkable applications in LIBs, solar energy, and supercapacitors due to their rich coordination chemistry of iron and sulfur.[155] Due to oxidation and reduction reactions in electrolytic conditions with polysulfide end constructions, iron holes surrounding sulfur lattices are particularly interesting to scientists. It might be a counter electrode for active electrochemical testing.[156,157] The mechanism of HER due to FeS has been shown in **Figure 7**.

7.1. Iron Sulfide-Based Nanocomposites for HER

Hosseini et al. reported that the goal is to develop new, easily fabricated structures to manufacture long-lasting, highly active electrocatalysts for the urea oxidation reaction (UOR) and HER. To achieve that Ni–S 3D patterns were studied.[158] In order to optimize the electrodeposition time, Ni–S 3D patterns were synthesized via gradient electrodeposition over four distinct time regimes. In order to improve the pulse electrodeposition parameters, Ni–Fe–S nanosheets were synthesized using pulse electrodeposition at three distinct frequencies and duty cycles. The sample produced at 13 min of gradient electrodeposition with a 1 Hz frequency and 0.7 duty cycle for pulse electrodeposition showed the greatest electrocatalytic performance. With just 54 mV and 1.25 V needed to give 10 mA cm^{-2} for HER and UOR reactions, respectively, the improved electrode demonstrated even more impressive performance. The two-electrode system's total cell voltage in 1 M KOH and 0.5 M urea was also measured at 1.313 V, yielding 10 mA cm^{-2}.

The electrochemical surface area of the Ni–S and Ni–S layers rose dramatically from 51 to 278 when Ni–Fe–S nanosheets were built over 3D Ni–S. The ideal Ni–Fe–S nanosheets on Ni–S had Tafel slopes of 131 mV dec^{-1} for the UOR and 98 mV dec^{-1} for the HER, respectively, and 182 mV dec^{-1} for the HER and UOR for the Ni–S coating layer. In terms of the HER and UOR, minimal variation in potential was seen at 100 mA cm^{-2} over 50 h, indicating remarkable electrocatalytic stability.[158]

Nourshargh et al. reported the first-ever electrochemical two-step synthesis of the NiFeS@CoFeLDH nanostructure. On the nickel foam (NF) substrate, the first layer of NiFeS was deposited in the first stage. In the second stage, the electrodeposition condition was controlled to deposit the second layer of cobalt–iron layered double hydroxide (CoFeLDH), on the first. Both the potential and the deposition duration were maximized. At current densities of −10 and −100 mA. cm^{-2}, respectively, the optimized NiFeS@CoFeLDH coating on NF displays minor overpotentials of −191.5 and −304.0 mV, indicating promising HER activity.

Moreover, the produced NiFeS@CoFeLDH electrocatalyst has excellent performance for the UOR because it requires just 358 mV overpotentials to function at a current density of 10 mA cm^{-2}. A highly steady response was seen for at least 10 h when the electrode stability was tested at an industrial scale current density of −100 and 10 mA. cm^{-2} for HER and UOR, respectively. The results demonstrated the synergistic impact of applying CoFeLDH and NiFeS electrocatalysts simultaneously, which enhances the active sites and raises the surface-to-volume ratio. Based on its excellent HER and UOR performance as well as its easy, quick, and binder-free production without requiring costly ingredients to build the electrocatalyst layer, the suggested electrode is a promising option for water splitting in the presence of urea.[159]

A simple synthetic procedure for synthesizing mesoporous FeS_2 without a rigid template (HER) was studied. Following a sulfurization process in a hydrogen sulfide environment, mesoporous FeS_2 materials with an extraordinary surface area were effectively produced using the sol-gel method. In their approach, outstanding HER catalytic performance was attained with an overpotential of 96 mV at 10 mA cm^{-2} of current and a Tafel slope of 78 mV per decade under alkaline conditions (pH 13). Exposed (210) facets are responsible for mesoporous FeS_2's high catalytic activity. As an alternative to Pt-based electrocatalysts for water splitting, the mesoporous FeS_2 material is cost-effective for HER.[160] Amorphous $Fe_{0.95}S_{1.05}$ nanorods are produced using a simple solvothermal process with an octylamine solvent and are used as a cheap and hyperactive electrocatalyst for an effective HER. In this process, molecules of capped octylamine formed the amorphous structure. Due to their irregular, chaotic atomic organization and abundance of unsaturated atoms, the alpha-FeS nanorods are endowed with many defects as exposed catalytic sites. The electrochemical active surface area and exceptional catalytic activity of alpha-FeS nanorods are significantly higher than those of crystalline $Fe_{0.95}S_{1.05}$ nanorods. A tiny Tafel slope of 43 mVdec^{-1}, low overpotential of 67 mV at the current density of 10 mA cm^{-2}, and lengthy operation stability of 80 h are significant results (**Figure 8a–d**). This study displays the
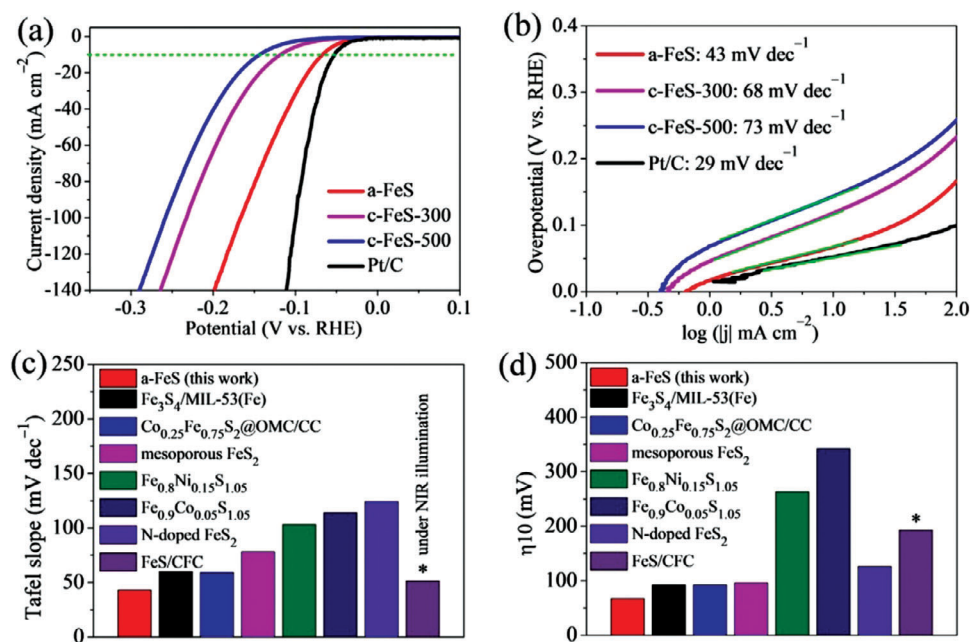
ADVANCED
SCIENCE NEWS
www.advancedsciencenews.com

NANO · MICRO
small
www.small-journal.com

Figure 8. a) Cathodic LSV curves of c-FeS-500, c-FeS-300, a-FeS, and Pt/C in 0.5 M H_2SO_4 electrolyte. b) Tafel plots of c-FeS-500, c-FeS-300, a-FeS, and Pt/C. c) Assessment of the overpotentials to drive a current density of 10 mA cm^{-2} of some recently reported iron sulfide-based catalysts. d) Comparison of the Tafel slopes of some recently reported iron sulfide-based catalysts. Reprinted with permission from.[161] Copyright 2022, American Chemical Society.

highest catalytic activity level for hydrogen production by FeS-based electrocatalysts.[161] While comparing mesoporous FeS_2 and amorphous $Fe_{0.95}S_{1.05}$ (a-FeS) nanorods, it was observed that the former has a lower overpotential than amorphous $Fe_{0.95}S_{1.05}$. The unique structure of iron sulfide resulted in enhanced HER properties vis reduced charge transfer resistance, lower Tafel slop and overpotential, increased electrochemical surface area, and improved stability. **Table 4**. depicts the comparison of various FeS-based nanocomposites for effective hydrogen evolution reactions.

8. Overall Water Splitting

Swathi et al. reported that transition metal sulfides are often used as bifunctional electrocatalysts because of their distinct structural characteristics, well-positioned active sites, and adjustable mechanical and electrical characteristics. Using a hydrothermal method, they have created very effective ternary copper iron sulfide ($CuFeS_2$)/reduced graphene oxide (rGO) composites for an overall water-splitting process. $CuFeS_2$ microflowers anchored on rGO sheets have their tetragonal structure determined by

Table 4. Comparison of various FeS-based nanocomposites for effective HER.

Composite	Tafel slope [mV dec^{-1}]	Overpotential [mV]	Current density [mA cm^{-2}]	Double-layer capacitance [mF cm^{-2}]	Resistance [Ω, ct]	Stability [h]	Synthetic method	Refs.
Fe–Mo–S/carbon nanocomposite	62	321	10	–	48	8000 s	Simple one-pot hydrothermal synthesis	[162]
PU@PANI@FeS$_2$	15	266	10	–	–	–	Electrospinning process.	[163]
Mesoporous FeS$_2$	78	96	10	·	238	24	Sol-gel method	[160]
alpha-FeS	43	67	10	8.7	5.5	80	Solvothermal method	[161]
g-C$_3$N$_4$/FeS$_2$/MoS	87.7	−193	10	20.9	0.961	10	Hydrothermal method.	[164]
FeS/Fe$_2$PeAg@IF	117.6	214.9	100	–	1.16	30	Two-step hydrothermal method	[165]
Ultra-thin troilite FeS nanosheets	36.9	142	10	–	14	100	Solvothermal process	[166]
Carbon-layer-coated CoS$_2$–FeS$_2$ heterojunction	105	210	10	4.1	–	26	A facile one-pot strategy	[167]
Fe$_3$O$_4$–FeS/IF	126.3	120.8	20	690.8	6	20	Chemical oxidation process	[168]
N–FeS$_2$	124	126	10	44	–	20	Facile solvothermal method	[169]

ADVANCED
SCIENCE NEWS
www.advancedsciencenews.com

NANO · MICRO
small
www.small-journal.com

X-ray analysis and compared to Joint Committee on Powder Diffraction Standards (JCPDS) #35−752. The presence of the rGO composite with $CuFeS_2$ is confirmed by the presence of two bands in the Raman spectrum: D (defects) and G (graphitic). The ratio of the D and G bands (I_D/I_G) is 1.18. The production of microflowers with rGO sheets is confirmed by the morphological examination performed with scanning electron microscopy and transmission electron microscopy. Energy-dispersive X-ray analysis was used to determine the elemental composition of $CuFeS_2$/rGO. The results showed a weight proportion of different compositions of Cu (18.07%), Fe (11.32%), S (13.88%), and C (56.74%). $CuFeS_2$/rGO composites also showed large pore volume, diameter, and surface area, measuring 0.162 mL g^{-1}, 2.471 nm, and 50.3 m^2 g^{-1}, respectively. The produced electrodes were investigated by the use of electrochemical characterization. In both OER (176 mV and 216 mV dec^{-1}) and HER (153 mV and 150 mV dec^{-1}), the obtained data unmistakably demonstrated low overpotential and low Tafel slope values. Furthermore, the composite that was created had low 1.59 V cell voltages, resulting in a more stable water-splitting process. It also demonstrated a faradaic efficiency of 95.5% for O_2 and 97.8% for H_2. As a result, the rGO composite in ternary metal sulfide is primarily responsible for enhancing the material's electrocatalytic activity, and the $CuFeS_2$/rGO composite shows promise as an electrode for the water-splitting process.[170]

Bhardwaj et al. reported that in the field of renewable energy technology, creating an efficient material for electrocatalytic and supercapacitor (SC) applications is the main focus. Here, we describe a straightforward hydrothermal process for creating cobalt–iron-based nanocomposites, followed by phosphorization and sulfurization. X-ray diffraction has been used to confirm the crystallinity of nanocomposites, demonstrating an improvement in crystalline nature from as-prepared to sulfurized to phosphorized. In contrast to the phosphorized CoFe-nanocomposite, which needs 240 mV to achieve 10 mA cm^{-2}, the as-synthesized CoFe-nanocomposite needs 263 mV overpotential for the OER. For the CoFe-nanocomposite, the HER shows an overpotential of 208 mV at 10 mA cm^{-2}. Furthermore, the data improved upon phosphorization, reaching 10 mA cm^{-2} at 186 mV. The as-synthesized nanocomposite has a specific capacitance (Csp) of 120 F g^{-1} at 1 A g^{-1}, a power density of 3752 W kg^{-1}, and a maximum energy density of 4.3 Wh kg^{-1}. Furthermore, with the maximum power and energy density of 4.2 kW kg^{-1} and 10.1 Wh kg^{-1}, as well as 252 F g^{-1} at 1 A g^{-1}, the phosphorized nanocomposite exhibits the best performance. This demonstrates that the outcomes are enhanced more than twofold. The 97% preservation of capacitance after 5000 cycles demonstrates the phosphorized CoFe's cyclic stability. Thus, their study provides highly efficient and cost-effective material for applications involving the generation and storage of energy.[171]

Due to its high metallic conductivity and low cost, iron–nickel sulfide is one of the most favorable bifunctional electrocatalysts for HER and OER in alkaline media. $(Ni, Fe)_3S_2$ has been reported to have some HER activity; however, this activity is currently lacking. A facile one-step simultaneous sulfuration and phosphorization technique was used to produce P-doped $(Ni, Fe)_3S_2$ nanosheet arrays on nickel foam that demonstrate significantly improved HER activity and drive outstanding

OER activity (**Figures 9** and **10**). The improvements in electrical conductivity and electrochemical surface area, as well as a notable optimization of the hydrogen/water absorption free energy (GH*/GH$_2$O*), can be attributed to P's integration. Overpotentials for HER and OER in 1 M KOH are similarly low for the optimum P–$(Ni, Fe)_3S_2$/NF, coming in at 98 and 196 mV at 10 mA cm^{-2}. In addition, the P–$(Ni, Fe)_3S_2$/NF electrodes used in an alkaline electrolyzer require just 1.54 V at 10 mA cm^{-2} in cell voltage, show excellent long-term stability, and are more effective than the vast majority of other modern electrocatalysts. Future applications of the disclosed electrocatalyst activation strategy by anion doping are very promising. This method can be applied to various transition metal chalcogenides for electrolysis.[172] Implementing commercial electrocatalytic water splitting cycles that produce clean hydrogen necessitates a scalable method for manufacturing stable bifunctional electrocatalysts. A 3D core chrysanthemum-like FeS/Ni_3S_2 heterogeneous nanoarray was effectively fabricated on a porous nickel foam skeleton using a modest and rapid one-step hydrothermal technique. With overpotentials of just 192 mV (−10) for OER and 130 mV for HER, chrysanthemum-shaped FeS/Ni_3S_2@NF heterostructure nanostructures demonstrate enhanced catalytic activity in alkaline environments. This research confirms that integrated interface engineering and accurate morphology control are efficient methods for accelerating the OER kinetics and strengthening the overall water-splitting performance by promoting charge transfer, activating the Ni^{3+}/Ni^{2+} coupling, and enhancing the material's intrinsic activity.[173] Various advanced iron sulfide-based nanocomposites for effective overall water splitting are depicted in **Tables 5** and **6**.

9. Supercapacitors

The rapid advancement of human civilization has resulted in environmental degradation and energy deficit. Consequently, there is a rising need for renewable and unpolluted energy resources, including wind power, hydropower, solar power, and biofuels.[183,184] As a result of their extreme reliance on environmental factors, significant effort is devoted to the research and development of efficient and practically applicable energy storage systems to meet the demands of energy sources globally.[185] The ongoing expansion of the human population is now dependent on fossil fuels. Renewable energy resources comprising wind, tidal, and sun have been widely utilized to achieve these increasing energy demands in recent years. Still, consumption rates have enhanced the need for efficient energy sources with sophisticated storage technologies.[186] Supercapacitors are gaining popularity because of their cheap maintenance costs, high power densities, quick charge/discharge rates, and long cycle life (>1 000 000 cycles) in this context, with other advantages such as these.[187–190] Energy is stored between an electrolyte and a solid electrode, and while several names have been developed for supercapacitors, essential functions persist the same. Since 1957, General Electric first demonstrated and patented supercapacitor technology, and research into and development of these devices have been a priority in academia and industry. The electrodes' large surface area and the dielectric separator's low thickness in a supercapacitor allow it to store and release much more energy than a regular capacitor.[191]
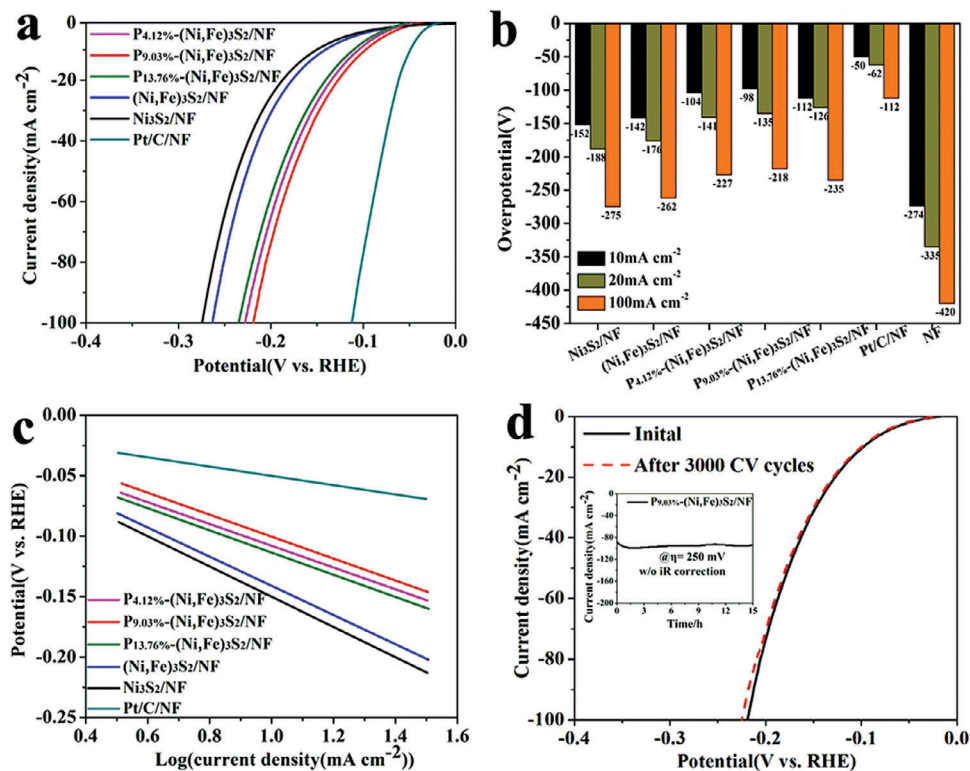
ADVANCED
SCIENCE NEWS

www.advancedsciencenews.com

NANO · MICRO
small
www.small-journal.com

Figure 9. a) LSV curves of Ni_3S_2/NF, $(Ni, Fe)_3S_2/NF$, $P_x\%-(Ni, Fe)_3S_2/NF$, and Pt/C/NF (x = 4.12, 9.03, and 13.76) evaluating HER performance. b) Comparison of overpotentials at 10, 20, and 100 mA cm^{-2}. c) Tafel plots. d) $P_{9.03\%}-(Ni, Fe)_3S_2/NF$ LSV curve after the first and 3000 cyclic voltammetry. Reprinted with permission.[172] Copyright 2019, American Chemical Society.
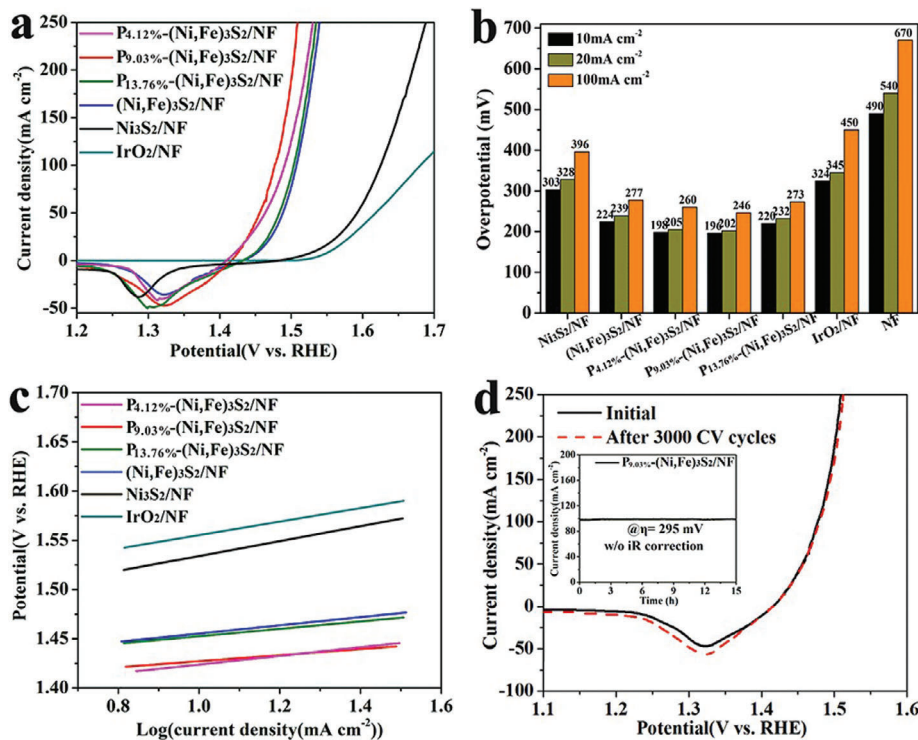
Figure 10. a) The LSV curves of the $(Ni,Fe)_3S_2/NF$, $P_{X\%}-(Ni, Fe)_3S_2/NF$, Ni_3S_2/NF, and IrO_2/NF of OER activity. b) The evaluation of overpotential at 10, 20, and 100 mA cm^{-2}. c) Tafel plots. d) The LSV curves of $P_{9.03\%}-(Ni, Fe)_3S_2/NF$ after the 1st, 3000th CV (Inset: Long-term stability test of $P_{9.03\%}-(Ni, Fe)_3S_2/NF$ at 295 mV [vs RHE]). Reprinted with permission.[172] Copyright 2019, American Chemical Society.

Table 5. Comparison of various FeS-based nanocomposites for effective water splitting (HER).

Composite	Tafel slope [mV dec^{-1}]	Overpotential [mV]	Current density [mA cm^{-2}]	Double-layer capacitance [mF cm^{-2}]	Resistance [ct, Ω]	Stability [h]	Synthetic method	Refs.
P–(Ni,Fe)$_3$S$_2$/NF	88	98 mV	10	18.7	1.56	15	A simple one-step simultaneous phosphorization	[172]
FeS$_2$	29.6	150	10	3.45	–	17	Hydrothermal	[174]
CoFeSP/CNT	67 (acidic) 70 (basic electrolyte)	114	10	13.9 (alkaline electrolyte) 11.3 (acidic electrolyte)	–	50	Three-step synthesis route	[175]
NiS$_2$/FeS$_2$/NC	68.56	172	10	6.3	–	8	Facile synthesis technique	[176]
H–Fe–CoMoS	58	138	10	79	–	20	Self–assembly approach	[177]
FeS/IF	77	243	100	–	2	100	Solvothermal system	[35]
Ni$_{0.7}$Fe$_{0.3}$S$_2$	109	155	10	3.0	–	50 000 s	Facile hydrothermal method	[178]
Ni–FeS/NF	29.6	157	10	0.040	–	11	One-pot electrodeposition process	[179]
FeS/Ni$_3$S$_2$@N	124	130	−10	22.8	2.6	55	One-step hydrothermal method	[173]
Ni$_{0.9}$Fe$_{0.1}$PS$_3$ nanosheets (NSs)	73	72	−10	2.74	5.6	50	Ultrasonication-assisted exfoliation process	[180]
Co$_{0.95}$Fe$_{6.05}$S$_8$	88	284	10	60	19	10	Two-step method	[181]

Supercapacitors have improved power densities compared to fuel cells and batteries, but they only store a fraction of the energy.[192] Researchers have focused on increasing the energy density of supercapacitors to match rechargeable batteries to close the power and energy gap between batteries and conventional capacitors.[193]

9.1. Performance Evaluation of Supercapacitors

High-performance supercapacitors have many desirable characteristics, such as excellent mechanical stability; large specific capacitances; outstanding cyclic lifespans; lower self-discharge rates; enormous power and high energy densities (> 10 Wh kg^{-1});

Table 6. Comparison of various FeS-based nanocomposites for effective water splitting (OER).

Composite	Tafel slope [mV dec^{-1}]	Overpotential [mV]	Current density [mA cm^{-2}]	Double-layer capacitance [mF cm^{-2}]	Resistance [ct, Ω]	Stability [h]	Synthetic method	Refs.
P–(Ni,Fe)$_3$S$_2$/NF	30	196	10	18.7	1.12	15	A simple one-step simultaneous phosphorization	[172]
FeS$_2$	29.6	326	100	3.45	–	17	Hydrothermal	[174]
CoFeSP/CNT	47	262	10	13.9 (alkaline electrolyte) 11.3 (acidic electrolyte)	–	12	Three-step synthesis route	[175]
NiS$_2$/FeS$_2$/NC	44.2	231	20	6.3	–	80	Facile synthesis technique	[176]
H–Fe–CoMoS	98	282	10	79	–	20	Self-assembly approach	[35]
FeS/IF	82.7	238	10	–	2 Ω	> 30	Solvothermal system	[178]
Ni$_{0.7}$Fe$_{0.3}$S$_2$	56	198	10	3.0	–	50 000 s	Facile hydrothermal method	[179]
Ni–FeS/NF	59.2	255	100	0.040	–	11	One-pot electrodeposition process	[173]
FeS/Ni$_3$S$_2$@N	70	192	10	22.8	2.2 Ω	55	One-step hydrothermal method,	[180]
(Ni$_{0.9}$Fe$_{0.1}$PS$_3$) nanosheets (NSs)	69	329	20	2.74	5.6 Ω	50	Ultrasonication-assisted exfoliation process	[181]
Co$_{0.95}$Fe$_{6.05}$S$_8$	50	311	10	60	19 Ω	10	Two-step method	[35]
NiS@FeS$_2$ nanocomposites	63	298	20	–	92 Ω	12	Solvothermal method	[182]

ADVANCED
SCIENCE NEWS

www.advancedsciencenews.com

NANO · MICRO

small

www.small-journal.com

Quicker charge/discharge rates; larger voltage windows; safer operations; reduced fundamental and maintenance costs.[194] The qualities of the three parts that make up a supercapacitor, the negative electrode, the positive electrode, and the separator, significantly impact the device's overall performance. A specific surface area in electrode materials or active masses is crucial since it can give electrolytes more active sites and boost capacitance.[195] Pore size distribution, the morphology of electroactive materials, electrical conductivity, and the inherent characteristics of electrolytes and separators are other significant performance-affecting characteristics. Additionally, the porous shape of active masses may boost surface areas, facilitate electrolyte access, and lessen electrochemical polarization. Micropores (> 2 nm) may hinder ion transport; in addition to their function as ion buffering reservoirs, macropores (> 50 nm) do not significantly contribute to larger surface areas, making pore size a crucial component in boosting capacitance. Therefore, pore diameters equal to or close to the size of ions may generate maximal specific capacitances.[196] The equation for Specific Conductance using CV curves and supercapacitors using galvanostatic charge/discharge slope is as follows (Equations (7) and (8)).[197] These two approaches may determine the specific capacitance of electrode materials Equations (8) and (9).

$$C_s = 1/\left(mv\left(V_f - V_i\right)\right) \int_{V_i}^{V_f} I\left(V\right) dV \tag{8}$$

$$C_s = \frac{I\Delta t}{m\Delta V} \tag{9}$$

where the specific capacitance, C_s, is measured in F g^{-1}, the active mass of the electrode material, m, is given in grams, the potential scan rate, Vv, is shown in volts per second per volt, the voltage window, $V = (V_f V_i)$, is given in volts, the instantaneous current, I, is given in amperes, and the discharge time, t, is shown in seconds. The energy density of supercapacitors is less than that of batteries, and increasing it to battery levels is difficult.[198] Here, the density of both power and energy are essential characteristics to assess supercapacitor performances, and they may be computed with the aid of the following equations.

$$E = \frac{CV^2}{2} = \frac{QV}{2} \tag{10}$$

$$P = \frac{V^2}{4R} \tag{11}$$

where C represents the specific conductance (F), V represents the cell's voltage, m represents the active mass, and E represents the corresponding series resistance (in ohms). Further, increasing the energy density of a supercapacitor cell requires increasing the specific conductance and the voltage while reducing the equivalent series resistance. The energy and power densities of supercapacitors are found to be proportional to the voltage square (Equations (10) and (11)), indicating that an increase in cell voltage may significantly boost the electrochemical performance. In this case, the voltages of the cell are primarily affected by intrinsic properties, that is, additional redox capacitance, specific surface area, and electrical conductivity, as well as pore size (e.g., the use of ionic/organic electrolytes in place

of aqueous electrolytes); thus, optimizing these properties may increase the voltage.[199] One can achieve higher specific capacitance values by producing nanostructured materials with larger optimized pore sizes and surface areas and maintaining electric conductivities.[200] This is because the electrolyte ions can access more of the material's active sites, leading to faster faradaic reactions. Ion diffusion resistance in electrodes, contact resistance between current collectors and electroactive material, and intrinsic and ionic resistance in electrolytes contribute to the equivalent series resistance.[201] Scientists demonstrated that ESR values might be reduced and power densities increased by directly depositing electroactive materials on conductive substrates like Cu or Ni foam.[202]

9.2. Factors Affecting Supercapacitors

Materials of an electrode and their reliability with suitable electrolyte conjugates utilized for various operations providing necessary loftier specific energy have an important impact on SC activity. To significantly impact the performance improvement of SCs, unique high-performance supercapacitor technology development requires the careful manufacturing of electrode material and the appropriate usage of electrolytes.[203–206] Effective impending SC electrodes on electrode materials with high theoretical capacitance, porosity, highly accessible electrochemical active sites, short diffusion routes, and strong electrical conductivity to ensure high performance and effective usage. Therefore, innovative electrode material design that is both sustainable and economical in shape and composition may be favorable to increased activity, and this is where energy research has been focusing over the last several years.[207–210] The selection of electrolytes is just as significant as the electrode materials regarding how much energy can be stored, how stable the system is, and how much power it can produce.[211,212] The performance of SCs may be negatively affected by the electrolyte parameters, such as their thermal stability, ionic conductivity, ionic radius, charge carrier mobility, and dielectric constant. Many studies have concentrated on synthesizing various electrolytes to improve the performance of SCs.[213] Choosing electrolytes carefully is essential, as many have undesirable properties.

Even though ionic liquids and organic electrolytes may be used to create a broad chance interval for the higher energy density of SC, their lower ionic conductivity can lead to far higher equivalent series resistances than those of aqueous electrolytes. However, whereas organic electrolytes may function across a broad temperature range, they also carry the danger of flammability.[214] However, ionic liquids save the day regarding security, as organic electrolytes and ionic liquids have lower ionic conductivities than regular aqueous electrolytes. Low-potential electrolysis windows in highly ion-conductive aqueous electrolytes limit available energy.[215] Although they are the wave of the future, all-solid-state, flexible SCs have poor mechanical and thermal stability. As shown in **Figure 11**, electrolytes have a noticeable effect on SC performance, making it critical to develop suitable electrolytes by understanding the compatibility between electrodes via experimental and theoretical study. Several variables influence the efficiency of an energy harvesting system,
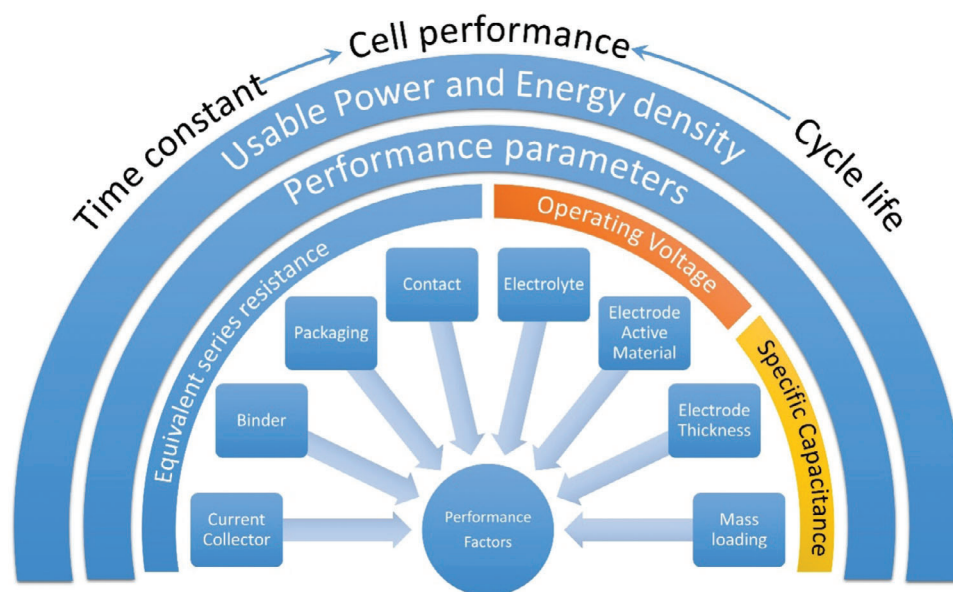
2402015 (16 of 30)

ADVANCED
SCIENCE NEWS
www.advancedsciencenews.com

NANO · MICRO
small
www.small-journal.com

Figure 11. Various factors affecting the performance of supercapacitors

including the materials used and the design of the accompanying energy storage system. Properties of material against the device's performance must be carefully addressed, as may the separator, packaging, and electrode thickness, which can considerably influence the time constant and total output of SCs.[216]

9.3. Iron Sulfide-Based Nanostructures as Effective Supercapacitors

Iron sulfide (FeS_2) has gained the attention of many researchers because of its potential use in energy storage applications. It is inexpensive, exhibits extremely strong electrical conductivity, and has abundant active sites.[49,217,218] Numerous supercapacitors with unique morphologies and architectures have been created using nanocomposites of FeS_2 as the electrode material. One example is the hydrothermal fabrication of a hybrid supercapacitor composed of FeS_2 and reduced graphene oxide. Under the same circumstances, the specific capacitance of the developed hybrid supercapacitor is 21.28 mF cm^{-2} higher than that of pure iron sulfide. In addition, after 10 000 cycles at a current density of 0.3 mA cm^{-2}, it still had 90% of its original SC.[219] Due to its low cost, high availability, abundance, benign nature, vast region having several electrochemically active sites, and a range of valences, iron sulfide has attracted significant attention as a possible electrode material for supercapacitor devices.[220,221] Iron sulfide and composite materials based on it have been the subject of several efforts at synthesis, with each shape chosen to meet the need for high energy density best. Karade et al. used a 2 V potential window to manufacture an asymmetrical supercapacitor device that can effectively bend in the solid state. The manufactured device had notable electrochemical features at a galvanostatic current of 0.75 mA, including an SC of 4.62 F g^{-1} and a high specific energy of 2.56 Wh kg^{-1}. The symmetric device showed excellent cyclic stability, with 91% capacitance retention after 1000 cycles and

bending the device up to 175 C. The potential usefulness of the solid-state devices was shown by lighting a panel of 21 red LEDs. Because of its high electrochemical characteristics, it was easily shown that it might be used in flexible, portable electronics.[222] Zardkhoshoui et al. created a positive electrode composed of graphene-wrapped $NiCo_2S_4$ microspheres on a nickel foam substrate and a negative electrode composed of petal-like FeS_2 on a nickel-foam substrate. Electrochemical testing found a large specific capacitance of 2112.30 F g^{-1} with a negligible loss of 6.8% after 5000 cycles. In addition, FeS_2 demonstrated a specific capacitance of 321.30 F g^{-1} with a respectable rate capacity of 47% capacitance retention. Graphene-wrapped $NiCo_2S_4$ microspheres and iron sulfide petals made up a flexible asymmetric device. Due to its notable electrochemical properties, it displayed a specific capacitance of 221.30 F g^{-1} and a remarkable energy density of 78.68 Wh kg^{-1}.[223] Chen, Shi, et al. developed an innovative hierarchical structure of $T/2HMoS_2$ nanoflower ornamented with watermelon-like FeS_2@carbon nanospheres using a simple synthetic approach. A standard three-electrode setup with 6M KOH electrolyte was used for the electrochemical performance. The specific capacitance of the synthesized composite hybrid materials was 1321.4 F g^{-1} at 2 A g^{-1}, with outstanding capacitance retention of 81.2% and cycling stability after 1000 cycles. Electrochemical characteristics suggested that the mesoporous structure of MoS_2, the carbon layer, and the FeS_2 all work together to make this material an excellent candidate for use as a supercapacitor electrode in future research.[224] Due to its remarkable performance as a supercapacitor electrode material, FeS^2/PVP/NF was produced using a simple and inexpensive chemical bath deposition process. With a specific capacitance of 526.08 F g^{-1} at a current density of 1 A g^{-1}, the composite material was an efficient electrode material for an SC when tested in a 3 M KOH solution. In addition, after 3000 charge–discharge cycles, it retained 91.2% of its original capacitance, demonstrating a remarkable rate capability far greater than that of naked FeS_2/NF. Due to its larger surface area, greater number of active

sites, and faster electron transfer and ion transport channel, the composite containing PVP exhibited improved electrochemical characteristics.[225] With simple reflux combined with an annealing technique, Liu et al. synthesized a hierarchical $Fe_3O_4@FeS_2$ nanocomposite as a high specific-capacitance electrode material for a supercapacitor. The charge may move more quickly between the electrode surface and the electrolyte due to the heterojunction between Fe_3O_4 and FeS_2. Excellent cycling stability and rate capability, as well as a high specific conductance of 597.1 F g^{-1} in 1 M potassium hydroxide at a current density of 3 A g^{-1}, showed that the produced sample was a good electrode material for future electrochemical energy storage devices.[226] Sun et al. manufactured phosphorous-doped FeS_2 grown over graphene as anode materials for a hybrid supercapacitor using a microwave-assisted method and a heat treatment with $NaH_2PO_2 2H_2O$. PSFG ($Pr_{0.8}Sr_{0.2}Fe_{0.8}Ga_{0.2}O_3$) material manufactured has a great surface area and good electrical conductivity. A three-electrode setup examined the PFSG's electrochemical performance in a 2M KOH of aqueous electrolytic solution. Over the potential range of 1.1 to 0 V, it displayed a high specific capacity of 246 mA h g^{-1} at a current density of 3 A g^{-1}. In addition, they produced a hybrid supercapacitor with PFSG serving as the anode and $Ni(OH)_2@Co_9S_8$ serving as the cathode, resulting in a superb energy density of 111 Wh kg^{-1} at an average power density of 1045 W kg^{-1}. The findings suggest they might be used in electrochemical storage systems.[227] The hierarchical nanostructure of $Fe_7S_8@Fe_5Ni_4S_8$ was synthesized by Zhang, Liu, et al. in a single alcohol thermal process, mimicking the structure of a flower's central stamen and outer petals. After undergoing a standard three-electrode electrochemical test, it was found that the material had a high specific capacitance of 670.4 F g^{-1} at a current density of 1 A g^{-1}, along with an excellent rate capability of 79.2%. A high energy density of 49.9 Wh kg^{-1} was achieved at a power density of 770.0 W kg^{-1} in a constructed asymmetric device with activated carbon serving as the cathode and $Fe_7S_8@Fe_5Ni_4S_8$ serving as the anode, and the device showed excellent long-term cycling stability.[228] Synthesis of $Fe_3O_4@FeS$ composites has been shown in this work using a simple and inexpensive solid-phase reaction and in situ growing procedure. This technology reduces the need for expensive FeS preparation while offering a novel approach to the wide-ranging use of acid-pickled iron oxide red. Lithium-ion batteries (LIBs) and supercapacitor electrodes made from $Fe_3O_4@FeS$ composites have high conductivity and good electrochemical performance far exceeding those of pure FeS. The synergistic interaction between Fe_3O_4 and FeS is crucial throughout the discharge process, and the structure's distinctive enhancements to FeS's electrochemical property and conductivity attest to this. For example, the kinetic study reveals that the electrode material contributes as much as 98.6% to the pseudo capacitance. The high specific energy of 64.6 Wh kg^{-1} is delivered by an all-solid-state hybrid supercapacitor made using $Fe_3O_4@FeS$ as the positive electrode, and the specific energy is maintained at 8000 W kg^{-1}.[229] Here, they used a double-substitution method using an anion and a cation to synthesize iron sulfide nanoparticles on a graphene composite with electrical conductivity improvements over pure FeS_2. The NiFeSP/G composite shows an amazing rate capability of 65% at 100 A g^{-1} and a high specific capacity of 765 C/gat 5 A g^{-1}. The NiFeSP/G anode and NiCo-

LDH/graphene cathode of an aqueous asymmetric supercapacitor exhibit a remarkable 109 Wh kg^{-1} at 1591 W kg^{-1} of energy density and a cycling performance of 89% after 8000 cycles.[230] Sun et al.[231] reported that biomass-based carbon electrode material with a hierarchical porous structure for supercapacitor applications is considered a viable option since it may improve electron transfer and shorten ion diffusion paths. However, their poor energy density severely limits the large range of uses of carbon-based materials. A straightforward pyrolysis procedure is used to create 3D N-doped hierarchical porous carbon combined with nickel–iron sulfide nanoparticles ($Fe_5Ni_4S_8$/FeS@N–HPC). There are additional channels for ion transport and electron transfer thanks to the 3D N-doped interconnected porous structure with a high specific surface area. To increase the charge storage capacity of supercapacitors, many sites for reduction and oxidation may occur inside the nickel–iron sulfide nanoparticles in the porous carbon. As a result, the $Fe_5Ni_4S_8$/FeS@N–HPC electrode that was produced shows remarkable electrochemical characteristics. At a current density of 0.5 A g^{-1}, the optimized $Fe_5Ni_4S_8$/FeS@N–HPC composite, which was manufactured below 800 °C, has an outstanding capacitance of 2812.4 F g^{-1} (734.56 C g^{-1}). Furthermore, the $Fe_5Ni_4S_8$/FeS@N–HPC-800/active carbon asymmetric supercapacitor exhibits a superior cycling stability of 93.24% over 10 000 charge–discharge cycles and an energy density of 76.8 Wh kg^{-1} at a power density of 395.03 W kg^{-1}.

Hassanpoor et al. reported that unique, simple, and effective procedures were used to produce tiny FeS_2 nanoparticles. In this work, graphene oxide was reduced and sulfur-doped simultaneously using a novel, straightforward chemical technique, resulting in the FeS_2-SRGO nanocomposite (pyrite–sulfur-doped reduced graphene oxide). Different physicochemical and electrochemical techniques were used to characterize and approve the prepared samples. On a carbon paste electrode substrate, the FeS_2-SRGO nanocomposite was coated. The electrochemical capacitive behavior of the electrode was investigated using the galvanostatic charge–discharge (GCD) method and CV in a variety of electrolytes, such as 6 M KOH, 1 M H_2SO_4, 1 M Na_2SO_4, 1 M NaCl, 1 M $NaNO_3$, 1 M KCl, and 3 M NaOH. The electrode in 1 M H_2SO_4 electrolyte with a specific capacity of 277 F g^{-11} has the highest supercapacitor performance, according to experimental data and specific capacitance calculations. Even after 200 charge and discharge cycles, the capacity retention remains at around 90% of the starting capacity.[232]

10. FeS as Effective Storage Material (LIBs and SIBs)

- Iron sulfides are plentiful and cheap, making them a suitable electrode material for energy storage applications. They play a crucial role as anodes in Li/Na battery technologies, as they have minimized electrolyte reduction, high Li/Na insertion voltages, and the development of solid electrolyte interface (SEI) layers. Like many other kinds of anode materials, iron sulfides have several drawbacks that must be addressed. Carbon-coated iron sulfides have been frequently used to improve their electrochemical characteristics to create nanostructures.[233,234] LIBs

ADVANCED
SCIENCE NEWS

www.advancedsciencenews.com

NANO · MICRO
small
www.small-journal.com

Table 7. Comparison of various iron sulfide-based materials for SIBs and LIBs.

Iron sulfide materials	Energy density	Power density	No. of cycles	Synthetic method	Application	Refs.
FeS/carbon microsphere	736 mAh g^{-1}	50 mA g^{-1}	50	Solvothermal method	SIBs	[236]
FeS$_2$ crystalline powder	420 mAh g^{-1}	0.1 C	30	Solid-state reaction	SIBs	[256]
FeS nanosheets/ultra-thin carbon	615 mAh g^{-1}	100 mA g^{-1}	100	Soft-template method	LIBs	[41]
FeS/rGO nanoparticle	978 mAh g^{-1}	100 mA g^{-1}	40	Direct precipitation and post-annealing	LIBs	[257]
FeS$_2$ nanocrystals (Li/Na)	(Na) 500 mAh g^{-1} (Li) > 630 mAh g^{-1}	1 mA g^{-1} and 0.3 mA g^{-1}	400 100	Solution-phase chemical synthesis	SIBs/LIBs	[258]
FeS$_2$/CPAN	470 mAh g^{-1}		50	Solid-state reaction	LIBs	[259]
FeS nano−structures/TiO$_2$	635 mAh g^{-1}	100 mA g^{-1}	100	Hydrothermal method	LIBs	[237]
FeS@C/carbon cloth (Li/Na)	(Li) 365 mAh g^{-1} (Na) 370 mAh g^{-1}	0.15 and 7.5 C.	100 50	Hydrothermal method	LIBs/SIBs	[42]
FeS nanodots @porous graphitic carbon nanowires	400 mAh g^{-1}	61 mA g^{-1}	50	Electrostatic spinning	LIBs	[260]
FeS$_2$ nanocrystals	401.7 mAh g^{-1}	0.5 mA g^{-1}	400	Solvothermal method	SIBs	[261]
FeS microsheet networks	677 mAh g^{-1}	100 mA g^{-1}	20	Hydrothermal method	LIBs	[262]
FeS/carbon nanofiber networks	535 mAh g^{-1}	1500 mA g^{-1}	200	Electrostatic spinning	LIBs	[263]
FeS$_2$−TFSI	542 Wh kg^{-1}	80% capacity retention	50	Ball-milled commercial FeS$_2$	LIBs	[264]
FeS nanoparticles/carbon nanosheets	703 mAh g^{-1}	1 A g^{-1}	150	Freeze-drying/carbonization method	LIBs	[41]
Sandwich graphene-wrapped FeS/graphene nanoribbons	536 mAh g^{-1}	400 mA g^{-1}	100	Chemical vapor deposition	SIBs/LIBs	[265]
FeS−N, S co-doped carbon nanostructures	1106.9 mAh g^{-1}	100 mA g^{-1} 500 mA g^{-1}	50	In situ growth	LIBs	[245]
Porous FeS nanofibers with numerous nanovoids (Na)	92 mAh g^{-1}	500 mA g^{-1}	150	Electrospinning and subsequent sulfidation	SIBs	[243]
FeS$_2$	415 mAh g^{-1}	200 mA g^{-1}	100	Solid-state method	SIBs	[266]
Yolk−shell FeS/C nanopheres (Na)	452 mAh g^{-1}	0.2 C	100	Solid-state method	SIBs	[242]
FeS/N, S-doped carbon	1106.9	1.1 mA g^{-1}	50	Carbonization	LIBs	[267]
Porous Co/FeS$_2$−C core/branch nanowire arrays	850 mAh g^{-1}		70	Chemical bath deposition, electrodeposition, and glucose decomposition	LIBs	[268]
Sandwiched graphene@FeS−graphene nanoribbons	693 mAh g^{-1}	0.1 mA g^{-1}	25	Vulcanization of graphene@Fe3O4−graphene nanoribbons via the CVD method	LIBs	[269]
Carbon precursor-coated FeS microcrystals	550		1st and 2nd	One-pot solvothermal reaction	LIBs	[270]
Pyrrhotite Fe−S@CNTs	674 mAh g^{-1} 670 mAh g^{-1}	50 mA g^{-1}	20th 65th	Vapor deposition and followed heat treatment	SIBs	[271]
FeS$_2$@rGO (SIBs)	240.5 mAh g^{-1} 192.9 mAh g^{-1}	250 mA g^{-1}		One-step hydrothermal method	SIBs	[272]
FeS/rGO-60	1300 mAh g^{-1}	1 A g^{-1}	1100	Hydrothermal method	LIBs	[273]
FeS/C@rGO	1428.2 mAh g^{-1}	0.1 A g^{-1}	130	Solvothermal and calcination	LIBs	[274]
FeS/MoS$_2$	325 mAh g^{-1}	5 A g^{-1}	200 cycles	Hydrothermal	SIBs	[275]
FeS@NSC composite	LIBs (185 mAh g^{-1}) SIBs (356.2 mAh g^{-1})	1 A g^{-1} 0.5 A g^{-1}	250 100	Solvothermal synthesis	LIBs/SIBs	[276]
FeS$_2$ nanorods	711.1 mAh g^{-1}	1000 mA g^{-1}	450	Facile chemical synthesis	SIBs	[277]
NiS−FeS@NC	395.8 mAh g^{-1}	1.0 A g^{-1}	200	Solvothermal	SIBs	[278]
FeS$_2$/SnS$_2$	Li (724.9 mAh g^{-1}) Na (451.8 mAh g^{-1})	02 A g^{-1} 0.2 A g^{-1}	500 200	Solvothermal	LIBs/SIBs	[279]
FeS@C	360 mAh g^{-1}	0.3 A g^{-1}	600	Sol−gel method	SIBS	[280]
FeS$_2$@Li$_2$S	360 mAh g^{-1}	1 A g^{-1}	100	Hydrothermal	SIBs	[281]
FeS$_2$@C	600.8 mAh g^{-1}	3A g^{-1}	1100	Solvothermal	SIBs	[282]
rGO@FeS$_2$@C	820.7 mAh g^{-1}	5 A g^{-1}	300	Hydrothermal	LIBs	[283]
S/FeS$_2$@CNTs	440.2 mAh g^{-1}	1 A g^{-1}	500	Facile chemical synthesis	LIBs	[284]

FeS has a substantially larger theoretical capacity (609 mAh g^{-1}) than commercial graphite (372 mAh g^{-1}) (Equation (12)).[235]

$$FeS + 2e^- + 2Li^+ - \longleftrightarrow Li_2S + Fe \qquad (12)$$
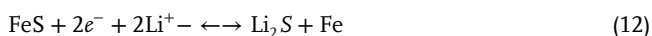
Many investigations have been conducted to determine how to enhance its electrochemical properties. The carbon nanosheet-encased FeS microspheres that Wu et al. produced exhibit impressive capacity and good high-rate capability.[236]

The battery has an initial capacity of 1564 mAh g^{-1} and retains 736 mAh g^{-1} after 50 cycles at 50 mA g^{-1}. The capacity drops to 541 mAh g^{-1} at 5 A g^{-1} reversible current from 783 mAh g^{-1} at a current density of 0.5 A g^{-1}, 734 mAh g^{-1} at 1 A g^{-1}, and so on. The dispersed presence of carbon nanosheets makes for enhanced performance. Polysulfides have more difficulty dissolving the FeS structure because of the carbon nanosheet wrapping. It has been shown that incorporating carbon nanosheets may significantly improve conductivity. Nanosheet-coated FeS (FeS@C) developed on carbon has the most significant material capacity at 1022 mAh g^{-1}.[41]

Because the SEI layer's charge capacity improves to 635 mAh g^{-1} after one cycle. The composite's ultra-thin thickness and tiny grains enhance the contact surface between the electrode material and the electrolyte, decreasing the path Li-ions take to diffuse through it. Also, after 20 cycles, its cycle capacity is 623 mAh g^{-1}; after 100 cycles, it drops to 615 mAh g^{-1}, which is constant. The addition of TiO$_2$ nanoparticles to FeS nanosheets was investigated.[237] FeS@TiO$_2$ nanostructures are much more cyclically stable than pure FeS, retaining 87% of their original capacity after 100 cycles and achieving a Columbic efficiency of 99%. The kinetics of Li-ion extraction and insertion at the electrolyte/electrode interface and the diffusion rate of Li-ion is improved by the presence of a TiO$_2$ phase. Wei et al. employed carbon-coated FeS as an anode without using carbon black or a current collector. The initial capacity is 453 mAh g^{-1} at 1.2 C, and after 200 cycles, only around 300 mAh g^{-1} remained.[42]

Capacity dropped from 560 mAh g^{-1} at 1.0–2.6 V to 370 mAh g^{-1} when the current density was raised from 0.15 to 7.5 C. By increasing the contact area between the electrolyte and electrode and decreasing the distance that electrons and ions must travel to reach the electrode, carbon cloth boosts cycle stability and rate performance. The carbon layer protecting FeS particles prevents the particles from clumping together and inhibits volume expansion during cycling. Deng et al. first reported synthesizing FeS/rGO nanocomposite and employing it as an anode in LIBs, demonstrating a specific capacitance of ≈432.9 mAh g^{-1}.[238] The composite's potential to exhibit superior electrochemical properties includes a high initial discharge capacity (1428.8 mAh g^{-1}). It is remarkable that after 150 cycles, the battery still has a 624.9 mAh g^{-1} capacity. It is also observed that adding carbon materials may protect the composite structure and improve experimental capability.

Each of the FeS mentioned above is a troilite. The possibility of Li storage in the uncommon pyrrhotite FeS has also been explored. Carbon nanotubes loaded with FeS nanoparticles were produced by Yu et al. At 50 mA g^{-1}, the 20th cycle capacity of the prepared Fe-S@CNTs was 674 mAh g^{-1}, while the 65th cycle capacity was 670 mAh g^{-1}.[41] Coating iron sulfide with the high

surface area graphitic biomass carbon improved the material's conductivity. It led to a discharge capacity of 505 mAh g^{-1} after 100 cycles at 1 C, despite iron sulfide's inherent weak structural and conductivity disorder during charge–discharge.[239] Luo et al. reported that after fully extracting two Li-ions, lithium iron silicate (Li$_2$FeSiO$_4$) has a high theoretical capacity of 332 mAhg^{-1} a considerable volume change, and a strong delithiation potential. Li$_2$FeSiO$_4$ cathode stabilization may be achieved by sulfur alteration. Through a hydrothermal and solid-state reaction pathway, a series of carbon-coated Li$_2$FeSiO$_4$ samples with various quantities of sublimed sulfur at 5, 10, 15, 20, and 25 at% were generated at a fixed sucrose content (14 wt% carbon). A thorough investigation was conducted into the crystal structures, chemical compositions, microstructures, and electrochemical performances of the various sulfur-modified Li$_2$FeSiO$_4$/C. Surface and near-bulk alterations of sulfur are examined, along with potential current chemical states of sulfur and sulfur–carbon co-modifications. All of the samples had a monoclinic P21 structure Li$_2$FeSiO$_4$, but the impure phases, iron sulfides (Fe$_{1-x}$S), and lithium metasilicate (Li$_2$SiO$_3$) were generated when the sulfur level exceeded 10%.

Furthermore, when sulfur and carbon were introduced to Li$_2$FeSiO$_4$ simultaneously, three different kinds of sulfur states were discovered. The sulfur–carbon co-modification would raise the charge transfer resistance while decreasing the resistance at the solid/electrode interface (SEI), as indicated by the surfaces' predominance of S–C and S–O–C. Increased interactions between sulfur and silicon S−Si(−O) or iron S−Fe(−S) close to the bulk might produce potential contaminants or sulfur replacing oxygen. While the latter is advantageous to increase specific capacity and cycle stability, the former is harmful since it lowers the effective sulfur quantity. The sulfur concentration of the sulfur–carbon co-modified sample has a complex effect on its overall performance. With 5 at% sulfur alteration, the highest initial discharge capacity of 152.3 mAhg^{-1} was achieved; with 15 at% sulfur modification, the greatest overall performance was noted, exhibiting a typical warm-up response and strong cycle stability.[240]

• Li et al. reported that because of its remarkable structure, high specific capacity, and changing chemical valence state, 2D layered marcasite (FeS$_2$) is a potential material for anode electrodes in LIBs. Nevertheless, there are significant volume variations throughout the discharge and charging operation, which causes a sharp decline in capacity and subpar electrochemical performance. The marcasite (FeS$_2$) anode's rapid electron transit would be greatly aided by introducing a sulfur vacancy structure, improving LIBs' electrochemical performance. Here, these issues were resolved using FeS$_2$ nanoparticles synthesized from the biomolecule L-cysteine as the sulfur source and the reduction process of GO to rGO sheets by NaBH$_4$, which resulted in an interesting S-vacancy 3D FeS$_2$/rGO (FSG) composite, guided by density functional theory (DFT) calculations. On the surface of rGO sheets, uniformly sized S-vacancy FeS$_2$ nanoparticles with an average size of 100 nm were generated. Comparing the FSG electrode to pure FeS$_2$, it exhibits a greater cyclability of 826 mAh g^{-1} after 150 cycles at 0.2 C and a higher rate capability of 410 mA h g^{-1} at 5 C (1 C = 900 mA g^{-1}). We demonstrate that S-vacancies may modify the surface electronic structure,

**ADVANCED
SCIENCE NEWS**

www.advancedsciencenews.com

NANO · MICRO

small

www.small-journal.com

increasing the binding energy and charge-transfer rate of FSG composites using DFT predictions and methodical characterization. We discovered that the substantial 3D and S-vacancy architectures of FSG anode materials account for their better performance. The FSG composite materials enhance the charge storage reversibility of the conversion process. The irreversible formation and breaking of Li–S bonds disintegrate the crystallographic structure. The findings show that a straightforward, workable process might be developed to create composites with an S-vacancy structure and high-performing anodes for LIBs.[241]

SIBs Na resources are both less expensive and more easily accessible than Li resources. Regarding theoretical capacity, FeS as an anode for SIBs is impressive, with an estimated 610 mAh g^{-1}. Yet, the shuttle effect of NaS$_x$ is substantial, leading to poor efficiency and rapid capacity decrease during operation at room temperature. Egg-shaped FeS@carbon nanospheres were produced.[242]

Due to the carbon shell's effect on the active material's conductivity, a high reversible capacity is achieved. By expanding the electrolyte/electrode contact and limiting the diffusion channel of ion/electron, nanosized FeS enhances the reaction rate by reducing the detrimental impact of volume changes during sodiation and desodiation and speeding up the reaction process. This battery has an impressive 722 mAh g^{-1} charge and discharge capacity right out of the box, and it maintains a steady 488 mAh g^{-1} at 0.2 C after 300 cycles. At 5 C, the rate can still achieve 452 mAh g^{-1} of capacity. Nanofibers of porous FeS were created.[243]

A high specific capacity of 283 mAh g^{-1} at a current density of 1 A/g was achieved after 400 cycles by Li et al. FeS nanoparticles decorate 1D carbon fiber for SIBs' excellent performance. It has been demonstrated that the strong 1D carbon support acts as a protective layer to stop the structural breakdown and loss of FeS active material, leading to increased throughput.[244]

Several other studies are being conducted on FeS anode materials with particular morphologies and remarkable electrochemical performance. The material and morphology of FeS, its synthetic technique, and electrochemical data are briefly addressed. Then, various carbon compounds coat or alter FeS materials, resulting in a diverse spectrum of hierarchical structures and morphologies. Also, the recent critical accomplishments in this area have helped make more precise comparisons between the varying electrochemical performances of FeS anode materials for LIBs.

11. FeS$_2$ as Effective Storage Material (LIBs & SIBs)

- There are many benefits to using FeS$_2$, such as its low toxicity, cheap cost, and natural abundance. Its appropriate band gap (Eg = 0.95 eV) makes it useful for solar cells. Electrochemical energy storage is another common use. In particular, the main Li/FeS$_2$ battery entered commercial use in the 1980s. Nevertheless, FeS$_2$ cannot be employed economically at room temperature because of its low electrochemical reversibility. Also, various researchers found a substantial discrepancy in the voltage profiles of FeS2 as an anode for LIBs.[245] LIBs

Four Li$^+$ ions may be stored per FeS$_2$ molecule by reacting to Li$_2$S and Fe. This gives the material a theoretical capacitance as large as 894 mAh g^{-1}, making it ideal for application in LIBs. Using carbon coating, Jin et al. created FeS$_2$ spheres on S-doped graphene (FeS$_2$@C/S–GAs).

$$FeS_2 + 4Li^+ + 4e^- \rightarrow 2Li_2S + Fe \quad (13)$$
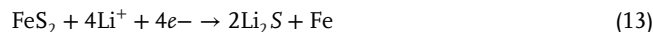
The initial anodic scan shows a single decrease peak at 1.15 V. The first cathodic scan reveals two peaks (at −1.94 and 2.55 V). The second reduction–oxidation cycle has a pair of oxidation peaks at −1.98 and 2.50 V and reduction peaks at −1.82 and 1.30 V. Due to the creation of the SEI layer and irreversible loss of electrolyte, FeS$_2$@C/S–GAs exhibits an extra peak at 0.64 V compared to pure FeS$_2$. Pure FeS$_2$ anodes often have poor rate capability and rapidly degrade capacity. Many techniques, including carbon coating and nanostructure preparation, have been undertaken to improve its poor conductivity and structural pulverization. Good electrochemical performance was achieved by creating water-soluble NaCl-templated FeS$_2$@C nanocomposites, and this was accomplished.[246]
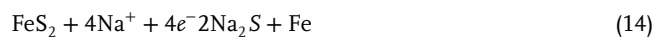
Creating the solid electrolyte interface (SEI) layers requires the irreversible consumption of lithium ions, contributing to the poor initial Columbic efficiency (70.8%). Yet, after being subjected to 300 milliampere seconds for 100 cycles, the composite has a 445.7 milliampere seconds per gram capacity. Furthermore, it shows excellent rate performance, with capacities of 440, 615, 720, and 820 mAh g^{-1} at 1000, 500, 300, and 200 mA g^{-1}, respectively. The "sphere on mattress" microstructure and design of FeS$_2$ sandwiched between carbons in the NaCl–FeS$_2$@C composite may boost conductivity and minimize polysulfide diffluence by boxing and absorbing. For their experiment, Du et al. used a solution route to synthesize rGO-wrapped FeS$_2$ microspheres that resemble cauliflower.[247]

After 700 cycles at 0.2 A g^{-1}, the anode's reversible capacity is 1720 mAh g^{-1}; after 800 cycles at 5.0 A g^{-1} and 85 °C, it drops to 340 mAh g^{-1}.

The regeneration of FeS$_2$ is a more favorable strategy for the full-charge reaction at the cathode, demonstrating comparatively strong cycling performance for the Li/FeS$_2$ battery, as indicated by a density functional theory simulation performed by Yamaguchi et al.[248]

- Numerous investigations have been conducted with pyrite-type FeS$_2$, but relatively few studies have been performed on the metastable marcasite form. Marcasite FeS$_2$'s electrochemical performance was investigated.[249] After 100 cycles at 0.1 A g^{-1}, the carbon nanofibers/FeS$_2$ composite maintains a capacity of 1399.5 mAh g^{-1}, at 10 A g^{-1}, its capacity drops to 782.2 mAh g^{-1}. Superior electrochemical performances are due to the hierarchical structures and the incorporation of carbon nanofibers, which enhance redox kinetics and structural stability.SIBs

According to the SIB theoretical capacity formula,

$$FeS_2 + 4Na^+ + 4e^- \rightarrow 2Na_2S + Fe \quad (14)$$

**ADVANCED
SCIENCE NEWS**
www.advancedsciencenews.com

**NANO · MICRO
small**
www.small-journal.com

FeS$_2$ has a capacity of 894 mAh g^{-1}. Clean FeS$_2$ as electrode materials for sodium ion batteries causes rapid capacity fading and low rate ability because its semiconductor features and shape are pulverized throughout the charging and discharging process. Polysulfides (Na$_2$S$_x$, $2 \leq x \leq 8$) may be dissolved in non-aqueous electrolytes at potentials below 0.8 V,[250] and their production decreases when FeS$_2$ is used. These problems may be solved by regulating the discharge cut-off voltage and obtaining nanostructured FeS$_2$ with a carbon covering.[251,252]

Electrolytes of the ether type, 1.0 M NaCF$_3$SO$_3$ in diglyme, were used instead of the more common carbonate type, and FeS$_2$ showed a significant improvement in its capacity to store Na.[253] An energy density of 750 Wh kg^{-1}, or more than 600 mAh g^{-1}, is possible at 20 mA g^{-1}. By increasing the current to 60 mA g^{-1}, the battery's capacity was raised to 530 mAh g^{-1}; after 100 cycles, 45% of its initial capacity remained. In addition to the research mentioned above, Kitajou et al. looked into the charge/discharge process of FeS$_2$ for SIBs.[254]

Using the high theoretical capacity of FeS$_2$, Chen et al successfully synthesized a juncus-based FeS$_2$/carbon/FeS$_2$ composite that demonstrated a high reversible capacity of 542.2 mAh g^{-1} at a current density of 0.1 A g^{-1}. The SEM reveals a reticulated structure, which slows the volume growth and facilitates rapid ion/electron kinetics, leading to increased Na$^+$ storage.[255] The summary of FeS and FeS$_2$ nanocomposite electrode materials for LIBs and SIBs is given in **Table 7**.

12. Summary of Prospects

Extensive analyses of various methods and approaches for preparing iron sulfide have been carried out. Scientists are particularly intrigued by metal sulfide materials because of their exceptional conductivity, specific surface area, lightweight, and expansive structure. These characteristics make them ideal electrode materials for electrocatalytic water splitting and supercapacitors. Iron sulfide has become increasingly popular among scientists studying hydrogen generation, oxygen evolution reaction, oxygen reduction reaction, and storage materials. This is due to its abundant supply, large specific surface area, excellent mechanical properties, and ease of molding. Scientists have made notable progress in improving the composition, structure, and control of the electrochemical performance of iron sulfide materials used in supercapacitors. These materials are often mixed with carbon-based, polymer-based, and semiconductor-based materials.

Nevertheless, there are still a multitude of issues and concerns that need more advancements and investigation. The fast evolution of society and the continual enhancement of nanomaterial preparation technology are causing people's expectations and requirements to increase. Hence, acquiring the knowledge to choose and fabricate iron sulfide-based nanomaterials and develop efficient, eco-friendly, smart, and economical techniques is crucial. Further inquiry is necessary to address specific difficulties identified via the description and analysis of prior research on iron sulfide materials in electrochemical water splitting and supercapacitors. Iron sulfide-based nanostructures are considered high-performance energy storage materials for supercapacitors and batteries because they possess improved electrical conductivity and specific surface area. The efficient performance of various nanocomposites based on iron sulfide is attributed to the synergistic interaction between FeS and other components. Among the various materials studied, Mo–FeS NSs exhibit a potential of 210 mV for the OER, alpha-FeS shows a potential of 67 mV for the HER, and FeS/G demonstrates a potential of 0.844 V for ORR. P-doped (Ni, Fe)$_3$S$_2$ displays potentials of 98 and 196 mV for HER and OER, respectively. Graphene-wrapped NiCo$_2$S$_4$ microspheres on an NF substrate and a negative electrode composed of petal-like FeS$_2$ exhibit a high specific capacitance of 2112 F g^{-1}. FeS/carbon microspheres demonstrate a high capacity of 736 mAh g^{-1} for SIBs, while FeS/C@rGO exhibits a 1428.2 mAh g^{-1} capacity for LIBs. Additional investigation in this domain using iron sulfide as a principal constituent can potentially facilitate the advancement of superior electrocatalysts and materials for energy storage.

Analysis of future directions of the research in this field highlights some important aspects.

1) The effect of structural design and material matching on the electrochemical performance was investigated in detail. Still, more research is required to evaluate iron sulfide's structural and synthesis properties and features. This study will help researchers fabricate various iron sulfide nanocomposites precisely.

2) The broader application of iron sulfide materials in energy production and storage depends on better balancing the interaction between the mechanical performance, electrochemical performance, and electrical conductivity of materials.

3) Researchers have long been concerned with the portability, lightweight stability, environmental adaptability, and safety of electrocatalysts, and these elements remain the focal points of future study and attention.

4) There are many unexplored fields of research into the interaction relationship, interface relationship, and synergistic effect of various components of iron sulfide composites. Finally, there is still a long way to go in researching and designing environmentally friendly, low-cost, and high-performance iron sulfide materials.

5) Efficient iron sulfide catalysts for water electrolysis may be developed with a better understanding of the reaction processes and active reaction centers.

6) FeS electrode materials can be improved by designing rational nanocomposites with desirable porosity and high specific surface area, mainly 3D hierarchical hollow/core–shell nanostructures, which could provide more extensive electrolyte/electrode interfaces, more active sites, and suppress the aggregation.

7) Researchers have paid much attention to experimental studies but have not explored much work on systematic theoretical studies. In order to forecast the structural connection and their performance and minimize synthesis iterations, we need advanced computational studies and designs for producing FeS electrode materials.

8) Since the iron component of FeS is connected to the redox stability and reactivity, it further impacts the electrochemical performances.

9) Altering composition is a straightforward technique to improve the electrochemical characteristics of FeS. Element doping, surface modification, and vacancies are successful

**ADVANCED
SCIENCE NEWS**

www.advancedsciencenews.com

NANO · MICRO

small

www.small-journal.com

10) Composite materials combining FeS with polymers, carbon materials (CNTs, graphene, etc.), and other metal-based materials (oxides, sulfides, etc.) have emerged as promising contenders for cutting-edge SCs. When combined with another material with inherent complementary qualities, the resulting composite structure has more flexibility, stability, and energy storage capacity.

11) FeS catalysts exhibit a lower susceptibility to sulfide poisoning compared to noble metal catalysts. Iron sulfide structures combined with 2D-carbon nanomaterials often demonstrate superior electrocatalytic activity and chemical durability compared to pure iron sulfides.

12) Similarly, additional metals or transition metal compounds doping the FeS phases result in the production of extremely reactive catalysts for energy storage materials.

13) In summary, these instances demonstrate the necessity for the advancement of novel electrocatalysts that contain FeS and the enhancement of current materials. This is crucial in order to fully use the untapped potential of a catalyst family that has been previously disregarded, specifically for the purpose of hydrogen evolution.

13. Conclusion

The article provides a summary of selected milestones in the fast-expanding research subject of developing iron sulfide catalysts for electrochemical hydrogen evolution. Despite being less advanced and generally less efficient than noble metal systems, iron sulfide electrocatalysts have shown remarkable catalytic efficacy in several well-designed materials. Specifically, the existence of disulfide groups (S_2^{2-}) contributes to a significant catalytic activity for the HER and OER, making FeS materials particularly appealing as electrocatalysts.

The quest for low-carbon (or non-carbon) energy has become more essential in energy engineering due to the ongoing use of fossil fuels and the more severe worldwide environmental pollution. Hydrogen referred to as "green energy," has enormous environmental benefits and possible practical uses, making it one of the most promising carbon-free energy sources. Among the available approaches, electrochemical water-splitting is a sustainable and cost-effective way to produce environmentally friendly green energy.

In electrochemical water splitting the catalyst's promotion of proton reduction with a low overpotential to reduce extra energy consumption is crucial for the efficiency and stability of the hydrogen evolution process. Because of this need, scientists are actively seeking ways to employ electrochemical catalysts for hydrogen production aiming to replace noble metal catalysts.

When considering electrocatalytic water splitting for hydrogen production, the pursuit of earth-abundant catalysts gained significant attention as electrocatalysts. The potential of metal sulfides, iron sulfide (Fe_xS_y), and multimetallic iron sulfide-based materials have been explored as electrocatalysts for HER, OER, ORR, and overall water splitting due to high their enhanced electrocatalytic activities and abundance concentrations of iron and sulfur in the Earth's continental crust to utilize in iron sulfide-based electrocatalysts development. Iron sulfide-based nanocomposites

such as Mo–FeS, alpha-FeS, and FeS/G have shown effective roles in OER, HER, and ORR respectively. TMSs have shown many advantageous features for electrocatalytic performance such as their weaker metal-sulfide ionic bonds, distinct structural characteristics, well-positioned active sites, and adjustable mechanical and electrical characteristics. Utilizing readily available and cost-effective materials for the development of electrocatalysts can pave the way for the sustainable production of hydrogen.

Besides water-splitting applications, iron sulfide-based nanostructures are also considered high-performance energy storage materials (supercapacitors and batteries) due to enhanced electrical conductivity and specific surface area. In order to provide electrolytes with more active sites and boost the capacitance, electrode materials with a high specific surface area are crucial. For high performance, supercapacitors should have desirable characteristics such as outstanding cyclic lifespans, faster charge/discharge rates, wider voltage windows, high energy densities, and excellent mechanical stability. Additionally, pore size distribution, morphology of electroactive materials, and electrical conductivity, are important features that impact performance. Various iron-sulfide-based nanocomposites showed efficient performance due to the synergistic interaction of other components with FeS. FeS/carbon microsphere and FeS/C@rGO are successfully employed for SIBs and LIBs, respectively. Carbon-coated iron sulfides have been also developed to improve their electrochemical characteristics.

However, for the large-scale application of Fe_xS_y-based electrocatalysts in sustainable hydrogen production via water splitting, or application in energy storage materials various factors including energy consumption, material consumption, and the generation of secondary waste, such as wastewater, and emissions during material development, should also be taken into account. Regarding practical usability, the durability of Fe_xS_y-based material is crucial for electrocatalytic water splitting or energy storage applications. Furthermore, when applying Fe_xS_y-based material on an industrial scale, considerations about the environmental impact of materials must be considered. A life cycle assessment (LCA) study could be beneficial to understanding the environmental aspect of Fe_xS_y-based material development and applications. Further research in this field using iron sulfide as a primary component can lead to the development of high-quality electrocatalysts and energy storage materials. When creating iron-sulfide-based energy storage or electrocatalysts materials additional crucial factors that must be taken into consideration are reduced fundamental and maintenance costs.

Conflict of Interest

The authors declare no conflict of interest.

Keywords

[1] M. Momirlan, T. Veziroglu, *Renewable Sustainable Energy Rev.* **2002**, *6*, 141.

[2] Z. Askarniya, X. Sun, Z. Wang, G. Boczkaj, *Chem. Eng. J.* **2023**, *454*, 140388.

[3] S. Shafiee, E. Topal, *Energy Policy* **2009**, *37*, 181.

[4] P. Fatehbasharzad, S. Aliasghari, I. S. Tabrizi, J. A. Khan, G. Boczkaj, *Water Resour. Ind.* **2022**, *28*, 100178.

[5] N. Sazali, *Int. J. Hydrogen Energy* **2020**, *45*, 18753.

[6] A. Farhan, M. Murad, W. Qayyum, A. Nawaz, M. Sajid, S. Shahid, M. A. Qamar, *J. Solid State Chem.* **2024**, *329*, 124445.

[7] M. Sajid, W. Qayyum, A. Farhan, M. A. Qamar, H. Nawaz, *Int. J. Hydrogen Energy* **2024**, *62*, 209.

[8] T. Reier, M. Oezaslan, P. Strasser, *ACS Catal.* **2012**, *2*, 1765.

[9] S. Fierro, T. Nagel, H. Baltruschat, C. Comninellis, *Electrochem. Commun.* **2007**, *9*, 1969.

[10] W. Hu, Y. Wang, X. Hu, Y. Zhou, S. Chen, *J. Mater. Chem.* **2012**, *22*, 6010.

[11] J.-X. Feng, S.-Y. Tong, Y.-X. Tong, G.-R. Li, *J. Am. Chem. Soc.* **2018**, *140*, 5118.

[12] H. Liang, A. N. Gandi, C. Xia, M. N. Hedhili, D. H. Anjum, U. Schwingenschlogl, H. N. Alshareef, *ACS Energy Lett.* **2017**, *2*, 1035.

[13] M. S. Burke, M. G. Kast, L. Trotochaud, A. M. Smith, S. W. Boettcher, *J. Am. Chem. Soc.* **2015**, *137*, 3638.

[14] Y. Ni, L. Yao, Y. Wang, B. Liu, C. Mao, C. Hu, *Nanoscale* **2017**, *9*, 11596.

[15] H. Sun, Y. Ye, Z. Tian, S. Wu, J. Liu, C. Liang, *RSC Adv.* **2017**, *7*, 49010.

[16] L. J. Foruzin, Z. Rezvani, Y. H. Shishavan, B. Habibi, *Int. J. Hydrogen Energy* **2018**, *43*, 150.

[17] S. Anantharaj, H. Sugime, S. Noda, *ACS Appl. Mater. Interfaces* **2020**, *12*, 27327.

[18] R. Elakkiya, G. Maduraiveeran, *Nanoscale* **2021**, *13*, 14837.

[19] S. Anantharaj, K. Karthick, S. Kundu, *Mater. Today Energy* **2017**, *6*, 1.

[20] J. Landon, E. Demeter, N. Inoglu, C. Keturakis, I. E. Wachs, R. Vasic, A. I. Frenkel, J. R. Kitchin, *ACS Catal.* **2012**, *2*, 1793.

[21] C. Zhang, B. Xin, S. Duan, A. Jiang, B. Zhang, Z. Li, J. Hao, *Chem Asian J* **2018**, *13*, 2700.

[22] J. Zhao, S. Xue, J. Barber, Y. Zhou, J. Meng, X. Ke, *J. Mater. Chem. A* **2020**, *8*, 4700.

[23] P. Ganesan, A. Sivanantham, S. Shanmugam, *J. Mater. Chem. A* **2016**, *4*, 16394.

[24] G. Qu, T. Wu, Y. Yu, Z. Wang, Y. Zhou, Z. Tang, Q. Yue, *Nano Res.* **2019**, *12*, 2960.

[25] C. S. Kim, S. H. Choi, J. H. Bang, *ACS Appl. Mater. Interfaces* **2014**, *6*, 22078.

[26] T. Guo, Y. Song, Z. Sun, Y. Wu, Y. Xia, Y. Li, J. Sun, K. Jiang, S. Dou, J. Sun, *J. Energy Chem.* **2020**, *42*, 34.

[27] J. Huang, J. Wen, G. Chen, W. Chen, G. Wang, H. Fan, D. Chen, C. Song, M. Li, X. Wang, *Appl. Catal., B* **2020**, *277*, 119220.

[28] J.-Y. Zhang, L. Lv, Y. Tian, Z. Li, X. Ao, Y. Lan, J. Jiang, C. Wang, *ACS Appl. Mater. Interfaces* **2017**, *9*, 33833.

[29] X. Zou, Y. Zhang, *Chem. Soc. Rev.* **2015**, *44*, 5148.

[30] M. Zeng, Y. Li, *J. Mater. Chem. A* **2015**, *3*, 14942.

[31] Q. Zhang, W. Chen, G. Chen, J. Huang, C. Song, S. Chu, R. Zhang, G. Wang, C. Li, K. K. Ostrikov, *Appl. Catal., B* **2020**, *261*, 118254.

[32] Y. Xiao, D. Su, X. Wang, S. Wu, L. Zhou, Y. Shi, S. Fang, H. M. Cheng, F. Li, *Adv. Energy Mater.* **2018**, *8*, 1800930.

[33] Y. Zhang, Q. Zhou, J. Zhu, Q. Yan, S. X. Dou, W. Sun, *Adv. Funct. Mater.* **2017**, *27*, 1702317.

[34] B. You, Y. Sun, *ChemPlusChem* **2016**, *81*, 1045.

[35] X. Zou, Y. Wu, Y. Liu, D. Liu, W. Li, L. Gu, H. Liu, P. Wang, L. Sun, Y. Zhang, *Chem* **2018**, *4*, 1139.

[36] S. Anantharaj, S. R. Ede, K. Sakthikumar, K. Karthick, S. Mishra, S. Kundu, *ACS Catal.* **2016**, *6*, 8069.

[37] W. M. Haynes, D. R. Lide, T. J. Bruno, *CRC Handbook of Chemistry and Physics*, CRC Press, Boca Raton, FL **2016**.

[38] D. Rickard, G. W. Luther, *Chem. Rev.* **2007**, *107*, 514.

[39] C. Zhao, X. Shao, Z. Zhu, C. Zhao, X. Qian, *Electrochim. Acta* **2017**, *246*, 497.

[40] C. Dong, X. Zheng, B. Huang, M. Lu, *Appl. Surf. Sci.* **2013**, *265*, 114.

[41] Y. Xu, W. Li, F. Zhang, X. Zhang, W. Zhang, C.-S. Lee, Y. Tang, *J. Mater. Chem. A* **2016**, *4*, 3697.

[42] X. Wei, W. Li, J.-A. Shi, L. Gu, Y. Yu, *ACS Appl. Mater. Interfaces* **2015**, *7*, 27804.

[43] M. Zhang, Z. Song, H. Liu, A. Wang, S. Shao, *J. Colloid Interface Sci.* **2021**, *584*, 418.

[44] L. Argueta-Figueroa, O. Martinez-Alvarez, J. Santos-Cruz, R. Garcia-Contreras, L. Acosta-Torres, J. De la Fuente-Hernandez, M. Arenas-Arrocena, *Mater. Sci. Eng., C* **2017**, *76*, 1305.

[45] R. S. Multani, K. E. Waters, *Can. J. Chem. Eng.* **2018**, *96*, 1185.

[46] Y. Xu, F. Bahmani, R. Wei, *Microsyst. Nanoeng.* **2020**, *6*, 1.

[47] K. Yang, G. Yang, L. Chen, L. Cheng, L. Wang, C. Ge, Z. Liu, *Biomaterials* **2015**, *38*, 1.

[48] R. Ahuja, A. Sidhu, A. Bala, *Eur. J. Plant Pathol.* **2019**, *155*, 163.

[49] S. Yu, V. M. H. Ng, F. Wang, Z. Xiao, C. Li, L. B. Kong, W. Que, K. Zhou, *J. Mater. Chem. A* **2018**, *6*, 9332.

[50] Y. Park, D. Faivre, *ChemPlusChem* **2022**, *87*, 202100457.

[51] M. Talaeizadeh, S. A. Seyyed Ebrahimi, P. Khosravi, B. Hamawandi, *Materials* **2022**, *15*, 6946.

[52] J. Zhou, L. Wu, J. Zhou, K. Liang, Y. Song, Y. Tian, Q. Zhang, X. Lan, *Fuel* **2019**, *255*, 115759.

[53] H. Qin, J. Jia, L. Lin, H. Ni, M. Wang, L. Meng, *Mater. Sci. Eng., B* **2018**, *236*, 104.

[54] M. R. Gao, J. Jiang, S. H. Yu, *Small* **2012**, *8*, 13.

[55] Y. Yuan, L. Wang, L. Gao, *Front. Chem.* **2020**, *8*, 818.

[56] T. Pasinszki, M. Krebsz, D. Chand, L. Kótai, Z. Homonnay, I. E. Sajó, T. Váczi, *J. Mater. Sci.* **2020**, *55*, 1425.

[57] F. King, *A review of the properties of pyrite and the implications for corrosion of the copper canister*, Technical report, SKB, Sweden, TR-13-19, **2013**.

[58] K. Simeonidis, S. Liébana-Viñas, U. Wiedwald, Z. Ma, Z.-A. Li, M. Spasova, O. Patsia, E. Myrovali, A. Makridis, D. Sakellari, *RSC Adv.* **2016**, *6*, 53107.

[59] Z. Liu, F. Hu, J. Xiang, C. Yue, D. Lee, T. Song, *Part. Part. Syst. Charact.* **2018**, *35*, 1800163.

[60] X. Zhang, J. Li, J. Li, L. Han, T. Lu, X. Zhang, G. Zhu, L. Pan, *Chem. Eng. J.* **2020**, *385*, 123394.

[61] W. T. Yao, H. Z. Zhu, W. G. Li, H. B. Yao, Y. C. Wu, S. H. Yu, *ChemPlusChem* **2013**, *78*, 723.

[62] D. Li, Y. Fang, X. Zhang, *ACS Appl. Mater. Interfaces* **2020**, *12*, 8989.

[63] R. Akram, J. Akhtar, H. R. Khan, M. Akhtar, M. A. Malik, N. Revaprasadu, Y. AlGhamdi, M. H. Bhatti, *Chem. Pap.* **2022**, *76*, 6371.

[64] J. Moore, E. Nienhuis, M. Ahmadzadeh, J. McCloy, *AIP Adv.* **2019**, *9*, 035012.

[65] W. Gao, Y. Tan, B. Wu, Y. Chen, Z. Hu, Y. Wang, Y. Wen, Z. Zhou, N. Zhou, *Sep. Purif. Technol.* **2022**, *297*, 121422.

[66] A. M. K. Pasha, M. Hosseini, A. Fakhri, V. K. Gupta, S. Agarwal, *J. Mol. Liq.* **2019**, *289*, 110950.

[67] A. Mirzaei, G. Neri, *Sens. Actuators, B* **2016**, *237*, 749.

[68] W. Yin, M. Liu, Y.-Y. Chen, Q.-Z. Yao, S.-Q. Fu, G.-T. Zhou, *Appl. Clay Sci.* **2022**, *228*, 106597.

[69] C. Ding, Y. Yan, D. Xiang, C. Zhang, Y. Xian, *Microchim. Acta* **2016**, *183*, 625.

[70] E. Myrovali, K. Papadopoulos, I. Iglesias, M. Spasova, M. Farle, U. Wiedwald, M. Angelakeris, *ACS Appl. Mater. Interfaces* **2021**, *13*, 21602.

2402015 (24 of 30)

**ADVANCED
SCIENCE NEWS**

www.advancedsciencenews.com

NANO · MICRO

small

www.small-journal.com

[71] A. Ridhova, V. Puspasari, M. I. Amal, in *Chalcogenide-Based Nanomaterials as Photocatalysts*, (Ed.: M. M. Khan), Elsevier, Amsterdam **2021**, pp. 105–134.

[72] W. Yang, C. Xiang, Y. Xu, S. Chen, W. Zeng, K. Liu, X. Jin, X. Zhou, B. Zhang, *Biomaterials* **2020**, *255*, 120186.

[73] A. D. Terna, E. E. Elemike, J. I. Mbonu, O. E. Osafile, R. O. Ezeani, *Mater. Sci. Eng., B* **2021**, *272*, 115363.

[74] Y.-Y. Liao, A. I. Huerta, J. B. Jones, M. L. Paret, in *Nanotechnology-Based Sustainable Alternatives for the Management of Plant Diseases*, (Eds.: G. M. Balestra, E. Fortunati), Elsevier, Amsterdam **2022**, pp. 243–252.

[75] T.-Y. Kim, M. G. Kim, J.-H. Lee, H.-G. Hur, *Front. Microbiol.* **2018**, *9*, 2817.

[76] Y. Shan, W. Lu, L. Xi, Y. Qian, *Front. Chem.* **2022**, *10*, 1000709.

[77] F. B. Mandal, *Isr. J. Ecol. Evol.* **2021**, *1*, 1.

[78] H. Zhang, Y. Cao, Y. Tian, L. Zheng, H. Huang, *Process Saf. Environ. Prot.* **2021**, *152*, 527.

[79] D. A. Bazylinski, *Int. Microbiol.* **1999**, *2*, 71.

[80] Y. Yang, T. Cheng, G. Zhou, *Geomicrobiol. J.* **2022**, *40*, 1.

[81] Q. Jin, J. Liu, W. Zhu, Z. Dong, Z. Liu, L. Cheng, *ACS Appl. Mater. Interfaces* **2018**, *10*, 332.

[82] A. Jin, M.-J. Kim, K.-S. Lee, S.-H. Yu, Y.-E. Sung, *Nano Res.* **2019**, *12*, 695.

[83] C. Panda, P. W. Menezes, *Angew. Chem., Int. Ed.* **2018**, *57*, 11130.

[84] H. Wendt, G. Imarisio, *J. Appl. Electrochem.* **1988**, *18*, 1.

[85] K. Zeng, D. Zhang, *Prog. Energy Combust. Sci.* **2010**, *36*, 307.

[86] Z. Yan, H. Liu, Z. Hao, M. Yu, X. Chen, J. Chen, *Chem. Sci.* **2020**, *11*, 10614.

[87] S. Anantharaj, S. Ede, K. Karthick, S. S. Sankar, K. Sangeetha, P. Karthik, S. Kundu, *Energy Environ. Sci.* **2018**, *11*, 744.

[88] H. Dau, C. Limberg, T. Reier, M. Risch, S. Roggan, P. Strasser, *ChemCatChem* **2010**, *2*, 724.

[89] J. M. Bockris, E. Potter, *J. Electrochem. Soc.* **1952**, *99*, 169.

[90] L. Zhang, Y. Qi, L. Sun, G. Chen, L. Wang, M. Zhang, D. Zeng, Y. Chen, X. Wang, K. Xu, *Appl. Surf. Sci.* **2020**, *512*, 145715.

[91] F. Zhou, Y. Zhou, G.-G. Liu, C.-T. Wang, J. Wang, *Rare Met.* **2021**, *40*, 3375.

[92] M. Batool, A. Hameed, M. A. Nadeem, *Coord. Chem. Rev.* **2023**, *480*, 215029.

[93] Y. Chen, Y. Fan, Z. Cui, H. Huang, D. Cai, J. Zhang, Y. Zhou, M. Xu, R. Tong, *Int. J. Hydrogen Energy* **2023**, *48*, 27992.

[94] J. Qian, X. Guo, T. Wang, P. Liu, H. Zhang, D. Gao, *Appl. Catal., B* **2019**, *250*, 71.

[95] Z. Zhang, Y.-P. Deng, Z. Xing, D. Luo, S. Sy, Z. P. Cano, G. Liu, Y. Jiang, Z. Chen, *ACS Nano* **2019**, *13*, 7062.

[96] H. Jiang, Y. Liu, W. Li, J. Li, *Small* **2018**, *14*, 1703739.

[97] Z. Shao, H. Meng, J. Sun, N. Guo, H. Xue, K. Huang, F. He, F. Li, Q. Wang, *ACS Appl. Mater. Interfaces* **2020**, *12*, 51846.

[98] S. Liu, Z. Wang, S. Zhou, F. Yu, M. Yu, C. Y. Chiang, W. Zhou, J. Zhao, J. Qiu, *Adv. Mater.* **2017**, *29*, 1700874.

[99] J. Sun, S. E. Lowe, L. Zhang, Y. Wang, K. Pang, Y. Wang, Y. Zhong, P. Liu, K. Zhao, Z. Tang, *Angew. Chem., Int. Ed.* **2018**, *57*, 16511.

[100] Z. Wang, J. Ang, B. Zhang, Y. Zhang, X. Y. D. Ma, T. Yan, J. Liu, B. Che, Y. Huang, X. Lu, *Appl. Catal., B* **2019**, *254*, 26.

[101] L. Yang, D. Wang, Y. Lv, D. Cao, *Carbon* **2019**, *144*, 8.

[102] P. Guo, Z. Wang, T. Zhang, C. Chen, Y. Chen, H. Liu, M. Hua, S. Wei, X. Lu, *Appl. Catal., B* **2019**, *258*, 117968.

[103] H. Yang, B. Wang, H. Li, B. Ni, K. Wang, Q. Zhang, X. Wang, *Adv. Energy Mater.* **2018**, *8*, 1801839.

[104] Q. Wang, Y. Lei, Z. Chen, N. Wu, Y. Wang, B. Wang, Y. Wang, *J. Mater. Chem. A* **2018**, *6*, 516.

[105] S. Yang, Q. He, C. Wang, H. Jiang, C. Wu, Y. Zhang, T. Zhou, Y. Zhou, L. Song, *J. Mater. Chem. A* **2018**, *6*, 11281.

[106] S. S. Shinde, C.-H. Lee, A. Sami, D.-H. Kim, S.-U. Lee, J.-H. Lee, *ACS Nano* **2017**, *11*, 347.

[107] Y. Tong, P. Chen, T. Zhou, K. Xu, W. Chu, C. Wu, Y. Xie, *Angew. Chem., Int. Ed.* **2017**, *56*, 7121.

[108] J. O. M. Bockris, *J. Chem. Phys.* **1956**, *24*, 817.

[109] B. E. Conway, J. O'M Bockris, *Modern Aspects of Electrochemistry*, Butterworths, London **1954**.

[110] H. Over, *Chem. Rev.* **2012**, *112*, 3356.

[111] N. B. Halck, V. Petrykin, P. Krtil, J. Rossmeisl, *Phys. Chem. Chem. Phys.* **2014**, *16*, 13682.

[112] J. Rossmeisl, A. Logadottir, J. K. Nørskov, *Chem. Phys.* **2005**, *319*, 178.

[113] Y. Zhang, S. Wei, P. Xing, L. Dai, Y. Wang, *J. Electroanal. Chem.* **2023**, *936*, 117323.

[114] G. Wang, C. Wang, L. Zhao, F. Qiao, X. Zhang, H. Wang, W. Wang, J. Yin, H. Zhou, X. Liu, *Fuel* **2023**, *341*, 127686.

[115] S. Deng, X. Zhang, Y. Zhang, J. Ye, B. Mei, S. Lin, *Int. J. Hydrogen Energy* **2024**, *51*, 550.

[116] X. He, X. Zhao, F. Yin, B. Chen, G. Li, H. Yin, *Int. J. Energy Res.* **2020**, *44*, 7057.

[117] H. Fan, Y. Ma, W. Chen, Y. Tang, L. Li, J. Wang, *J. Alloys Compd.* **2022**, *894*, 162533.

[118] S. Zhang, Y. Sun, F. Liao, Y. Shen, H. Shi, M. Shao, *Electrochim. Acta* **2018**, *283*, 1695.

[119] X. Li, G. Zhu, L. Xiao, Y. Liu, Z. Ji, X. Shen, L. Kong, S. A. Shah, *J. Alloys Compd.* **2019**, *773*, 40.

[120] R. Zhang, Z. Hu, T. Ning, N. Chen, Z. Shang, M. He, J. Wu, H. Shi, *Colloids Surf. A* **2022**, *648*, 129181.

[121] W. Yang, G. Ma, Y. Fu, K. Peng, H. Yang, X. Zhan, W. Yang, L. Wang, H. Hou, *Chem. Eng. J.* **2022**, *429*, 132381.

[122] Y. Tan, X. Xu, Q. Li, X. Chen, Q. Che, Y. Chen, Y. Long, *J. Colloid Interface Sci.* **2021**, *594*, 575.

[123] G. Zhang, Z. Hao, J. Yin, C. Wang, J. Zhang, Z. Zhao, D. Wei, H. Zhou, Z. Li, *Dalton Trans.* **2020**, *49*, 9804.

[124] B. Wang, Y. Hu, B. Yu, X. Zhang, D. Yang, Y. Chen, *J. Power Sources* **2019**, *433*, 126688.

[125] Q.-W. Chen, X.-Y. Zhang, Y.-W. Dong, B.-Y. Guo, Y. Ma, L. Wang, R.-Q. Lv, Y.-L. Zhou, Y.-M. Chai, B. Dong, *J. Alloys Compd.* **2020**, *835*, 155298.

[126] M. Winter, R. J. Brodd, *Chem. Rev.* **2004**, *104*, 4245.

[127] X. Li, Q. Jiang, S. Dou, L. Deng, J. Huo, S. Wang, *J. Mater. Chem. A* **2016**, *4*, 15836.

[128] H. Yang, Y. Zhang, F. Hu, Q. Wang, *Nano Lett.* **2015**, *15*, 7616.

[129] Y. Liang, Y. Li, H. Wang, J. Zhou, J. Wang, T. Regier, H. Dai, *Nat. Mater.* **2011**, *10*, 780.

[130] S. Lee, G. Nam, J. Sun, J. S. Lee, H. W. Lee, W. Chen, J. Cho, Y. Cui, *Angew. Chem.* **2016**, *128*, 8741.

[131] H. Wang, Y. Liang, Y. Li, H. Dai, *Angew. Chem.* **2011**, *123*, 11161.

[132] J. Wang, L. Li, X. Chen, Y. Lu, W. Yang, *J. Mater. Chem. A* **2016**, *4*, 11342.

[133] C. Zeng, H. Huang, T. Zhang, F. Dong, Y. Zhang, Y. Hu, *ACS Appl. Mater. Interfaces* **2017**, *9*, 27773.

[134] Q. Huang, Q. Liu, L. Lin, F.-J. Li, Y. Han, Z.-G. Song, *Ecotoxicol. Environ. Saf.* **2018**, *159*, 261.

[135] M. Seredych, E. Rodriguez-Castellon, T. J. Bandosz, *J. Mater. Chem. A* **2014**, *2*, 20164.

[136] K. Cho, S. H. Han, M. P. Suh, *Angew. Chem.* **2016**, *128*, 15527.

[137] A. Bar-Hen, R. Bar-Ziv, T. Ohaion-Raz, A. Mizrahi, S. Hettler, R. Arenal, M. B. Sadan, *Chem. Eng. J.* **2021**, *420*, 129771.

[138] J. Yin, Y. Li, F. Lv, Q. Fan, Y.-Q. Zhao, Q. Zhang, W. Wang, F. Cheng, P. Xi, S. Guo, *ACS Nano* **2017**, *11*, 2275.

[139] L. An, W. Huang, N. Zhang, X. Chen, D. Xia, *J. Mater. Chem. A* **2014**, *2*, 62.

ADVANCED
SCIENCE NEWS

www.advancedsciencenews.com

NANO · MICRO

small

www.small-journal.com

[140] Y. Guo, H. Huang, Y. He, N. Tian, T. Zhang, P. K. Chu, Q. An, Y. Zhang, *Nanoscale* **2015**, *7*, 11702.

[141] J. Gautam, D. T. Tran, T. I. Singh, N. H. Kim, J. H. Lee, *J. Power Sources* **2019**, *427*, 91.

[142] X. Liu, Z. Xiao, J. Ren, F. Wang, C. Wei, Q. Xing, W. Yan, X. Li, Y. Chen, *Appl. Surf. Sci.* **2022**, *580*, 152255.

[143] R. Jiang, X. Chen, J. Deng, T. Wang, K. Wang, Y. Chen, J. Jiang, *J. Energy Chem.* **2020**, *47*, 79.

[144] H. Fang, T. Huang, J. Mao, S. Yao, M. M. Dinesh, Y. Sun, D. Liang, L. Qi, J. Yu, Z. Jiang, *ChemistrySelect* **2018**, *3*, 10418.

[145] S. N. Bhange, R. Soni, G. Singla, T. Ajithkumar, S. Kurungot, *ACS Appl. Nano Mater.* **2020**, *3*, 2234.

[146] H.-C. Huang, C.-Y. Su, K.-C. Wang, H.-Y. Chen, Y.-C. Chang, Y.-L. Chen, K. C.-W. Wu, C.-H. Wang, *ACS Sustainable Chem. Eng.* **2019**, *7*, 3185.

[147] O. Diaz-Morales, F. Calle-Vallejo, C. de Munck, M. T. Koper, *Chem. Sci.* **2013**, *4*, 2334.

[148] E. Gileadi, *Physical Electrochemistry, Fundamentals, Techniques and Applications*, Wiley-VCH Verlag GmbH & Co. KGaA, Weinheim **2011**, pp. 151–164.

[149] Y. Zheng, Y. Jiao, A. Vasileff, S. Z. Qiao, *Angew. Chem., Int. Ed.* **2018**, *57*, 7568.

[150] C. Hu, L. Zhang, J. Gong, *Energy Environ. Sci.* **2019**, *12*, 2620.

[151] T. Yu, Q. Xu, G. Qian, J. Chen, H. Zhang, L. Luo, S. Yin, *ACS Sustainable Chem. Eng.* **2020**, *8*, 17520.

[152] F. Xu, G. Qian, W. Chen, L. Luo, F. Shen, S. Yin, *J. Phys. Chem. C* **2020**, *124*, 19595.

[153] L. Chen, X. Dong, Y. Wang, Y. Xia, *Nat. Commun.* **2016**, *7*, 1.

[154] C. J. Raj, K. Prabakar, A. D. Savariraj, H.-J. Kim, *Electrochim. Acta* **2013**, *103*, 231.

[155] C. Zhao, G. Burrell, A. A. Torriero, F. Separovic, N. F. Dunlop, D. R. MacFarlane, A. M. Bond, *J. Phys. Chem. B* **2008**, *112*, 6923.

[156] M. G. Walter, E. L. Warren, J. R. McKone, S. W. Boettcher, Q. Mi, E. A. Santori, N. S. Lewis, *Chem. Rev.* **2010**, *110*, 6446.

[157] C. J. Raj, B. C. Kim, W.-J. Cho, W.-G. Lee, Y. Seo, K.-H. Yu, *J. Alloys Compd.* **2014**, *586*, 191.

[158] M. Hosseini, T. Shahrabi, G. B. Darband, A. Fathollahi, *Langmuir* **2024**, *40*, 2028.

[159] B. Noursharg, A. Ghaffarinejad, G. B. Darband, *J. Environ. Chem. Eng.* **2024**, *12*, 111629.

[160] R. Miao, B. Dutta, S. Sahoo, J. He, W. Zhong, S. A. Cetegen, T. Jiang, S. P. Alpay, S. L. Suib, *J. Am. Chem. Soc.* **2017**, *139*, 13604.

[161] J. Zhang, Y. Wu, H. Hao, Y. Zhang, X. Chen, K. Xing, J. Xu, *Electrochim. Acta* **2022**, *402*, 139554.

[162] Z. Huang, Z. Yang, M. Z. Hussain, Q. Jia, Y. Zhu, Y. Xia, *J. Mater. Sci. Technol.* **2021**, *84*, 76.

[163] C. Manjunatha, R. S. Patil, M. Sudeep, N. Srinivasa, R. C. Kumar, M. S. Aan, S. Ashoka, *Surf. Interfaces* **2020**, *18*, 100445.

[164] A. Nazir, A. Akbar, H. B. Baghdadi, S. ur Rehman, E. Al-Abbad, M. Fatima, M. Iqbal, N. Tamam, N. Alwadai, M. Abbas, *Arabian J. Chem.* **2021**, *14*, 103251.

[165] M.-X. Li, Y.-N. Zhou, Y.-W. Dong, X. Liu, R.-N. Luan, B. Liu, J.-B. Zeng, Y.-M. Chai, B. Dong, *Int. J. Hydrogen Energy* **2022**, *47*, 20518.

[166] G. Zhou, Y. Shan, L. Wang, Y. Hu, J. Guo, F. Hu, J. Shen, Y. Gu, J. Cui, L. Liu, *Nat. Commun.* **2019**, *10*, 1.

[167] W. Wang, Y. Xu, J. Yao, X. Liu, Z. Yin, Z. Li, *Dalton Trans.* **2020**, *49*, 13352.

[168] M. Yang, W.-H. Hu, M.-X. Li, Y.-N. Cao, B. Dong, Y. Ma, H.-Y. Zhao, F.-G. Wang, J. Huang, Y.-M. Chai, *J. Energy Chem.* **2022**, *68*, 96.

[169] J. Ye, Y. Zang, Q. Wang, Y. Zhang, D. Sun, L. Zhang, G. Wang, X. Zheng, J. Zhu, *J. Energy Chem.* **2021**, *56*, 283.

[170] S. Swathi, R. Yuvakkumar, G. Ravi, M. Thambidurai, H. D. Nguyen, D. Velauthapillai, *ACS Appl. Nano Mater.* **2023**, *6*, 6538.

[171] S. Bhardwaj, R. Srivastava, T. Mageto, M. Chaudhari, A. Kumar, J. Sultana, S. R. Mishra, F. Perez, R. K. Gupta, *Discover Nano* **2023**, *18*, 59.

[172] C. Liu, D. Jia, Q. Hao, X. Zheng, Y. Li, C. Tang, H. Liu, J. Zhang, X. Zheng, *ACS Appl. Mater. Interfaces* **2019**, *11*, 27667.

[173] H. Li, S. Yang, W. Wei, M. Zhang, Z. Jiang, Z. Yan, J. Xie, *J. Colloid Interface Sci.* **2022**, *608*, 536.

[174] S. Shit, P. Samanta, S. Bolar, N. C. Murmu, P. Khanra, T. Kuila, *Bull. Mater. Sci.* **2021**, *44*, 1.

[175] L. Huang, H. Wu, H. Liu, Y. Zhang, *Electrochim. Acta* **2019**, *318*, 892.

[176] S. Wang, P. Ning, S. Huang, W. Wang, S. Fei, Q. He, J. Zai, Y. Jiang, Z. Hu, X. Qian, *J. Power Sources* **2019**, *436*, 226857.

[177] Y. Guo, X. Zhou, J. Tang, S. Tanaka, Y. V. Kaneti, J. Na, B. Jiang, Y. Yamauchi, Y. Bando, Y. Sugahara, *Nano Energy* **2020**, *75*, 104913.

[178] J. Yu, G. Cheng, W. Luo, *J. Mater. Chem. A* **2017**, *5*, 15838.

[179] S. Shit, S. Bolar, N. C. Murmu, T. Kuila, *ACS Sustainable Chem. Eng.* **2019**, *7*, 18015.

[180] B. Song, K. Li, Y. Yin, T. Wu, L. Dang, M. Cabán-Acevedo, J. Han, T. Gao, X. Wang, Z. Zhang, *ACS Catal.* **2017**, *7*, 8549.

[181] Y. Wu, Z. Meng, X. Fang, Y. Li, J. Bao, C. Zhang, Y. Wang, H. Tian, W. Zheng, *Ceram. Int.* **2021**, *47*, 26484.

[182] B. J. Rani, P. A. Kanjana, G. Ravi, R. Yuvakkumar, B. Saravanakumar, *Mater. Sci. Semicond. Process.* **2019**, *101*, 174.

[183] X. Sun, S. Liu, X. Zhang, Y. Tao, G. Boczkaj, J. Y. Yoon, X. Xuan, *Bioresour. Technol.* **2022**, *345*, 126251.

[184] E. Cako, Z. Wang, R. Castro-Muñoz, M. P. Rayaroth, G. Boczkaj, *Ultrason. Sonochem.* **2022**, *88*, 106081.

[185] J. Han, W. Wei, C. Zhang, Y. Tao, W. Lv, G. Ling, F. Kang, Q.-H. Yang, *Electrochem. Energy Rev.* **2018**, *1*, 139.

[186] D. P. Dubal, N. R. Chodankar, D.-H. Kim, P. Gomez-Romero, *Chem. Soc. Rev.* **2018**, *47*, 2065.

[187] Q. Song, Y. Li, S. Chan, *J. Appl. Electrochem.* **2005**, *35*, 157.

[188] J. Yuan, S. Tang, Z. Zhu, X. Qin, R. Qu, Y. Deng, L. Wu, J. Li, G. M. Haarberg, *J. Mater. Sci.: Mater. Electron.* **2017**, *28*, 18022.

[189] S. Natarajan, M. Ulaganathan, V. Aravindan, *J. Mater. Chem. A* **2021**, *9*, 15542.

[190] S. Khokhar, H. Anand, P. Chand, *J. Energy Storage* **2022**, *56*, 105897.

[191] M. Z. Iqbal, U. Aziz, *J. Energy Storage* **2022**, *46*, 103823.

[192] T. Wang, H. C. Chen, F. Yu, X. Zhao, H. Wang, *Energy Storage Mater.* **2019**, *16*, 545.

[193] L. Lyu, K.-d. Seong, D. Ko, J. Choi, C. Lee, T. Hwang, Y. Cho, X. Jin, W. Zhang, H. Pang, *Mater. Chem. Front.* **2019**, *3*, 2543.

[194] A. G. Olabi, M. A. Abdelkareem, T. Wilberforce, E. T. Sayed, *Renewable Sustainable Energy Rev.* **2021**, *135*, 110026.

[195] G. Wang, L. Zhang, J. Zhang, *Chem. Soc. Rev.* **2012**, *41*, 797.

[196] T. M. Gür, *Energy Environ. Sci.* **2018**, *11*, 2696.

[197] F. Wang, X. Wu, X. Yuan, Z. Liu, Y. Zhang, L. Fu, Y. Zhu, Q. Zhou, Y. Wu, W. Huang, *Chem. Soc. Rev.* **2017**, *46*, 6816.

[198] J. Yan, Q. Wang, T. Wei, Z. Fan, *Adv. Energy Mater.* **2014**, *4*, 1300816.

[199] C. Zhong, Y. Deng, W. Hu, J. Qiao, L. Zhang, J. Zhang, *Chem. Soc. Rev.* **2015**, *44*, 7484.

[200] Q. Wang, J. Yan, Z. Fan, *Energy Environ. Sci.* **2016**, *9*, 729.

[201] H. Shao, Y.-C. Wu, Z. Lin, P.-L. Taberna, P. Simon, *Chem. Soc. Rev.* **2020**, *49*, 3005.

[202] M. Yaseen, M. A. K. Khattak, M. Humayun, M. Usman, S. S. Shah, S. Bibi, B. S. U. Hasnain, S. M. Ahmad, A. Khan, N. Shah, *Energies* **2021**, *14*, 7779.

[203] P. K. Panda, A. Grigoriev, Y. K. Mishra, R. Ahuja, *Nanoscale Adv.* **2020**, *2*, 70.

[204] L. Zhang, S. Yang, J. Chang, D. Zhao, J. Wang, C. Yang, B. Cao, *Front. Chem.* **2020**, *8*, 413.

[205] S. Manoharan, K. Krishnamoorthy, A. Sathyaseelan, S.-J. Kim, *Mater. Chem. Front.* **2021**, *5*, 6200.

**ADVANCED
SCIENCE NEWS**

www.advancedsciencenews.com

**NANO · MICRO
small**

www.small-journal.com

[206] S. Khasim, A. Pasha, N. Badi, M. Lakshmi, Y. K. Mishra, *RSC Adv.* **2020**, *10*, 10526.

[207] J. Shi, B. Jiang, C. Li, F. Yan, D. Wang, C. Yang, J. Wan, *Mater. Chem. Phys.* **2020**, *245*, 122533.

[208] P. Naskar, A. Maiti, P. Chakraborty, D. Kundu, B. Biswas, A. Banerjee, *J. Mater. Chem. A* **2021**, *9*, 1970.

[209] K. Nasrin, V. Sudharshan, K. Subramani, M. Sathish, *Adv. Funct. Mater.* **2022**, *32*, 2110267.

[210] B. N. Bhadra, Y. S. Baek, S. Kim, C. H. Choi, S. H. Jhung, *Appl. Catal., B* **2021**, *285*, 119842.

[211] B. Pal, S. Yang, S. Ramesh, V. Thangadurai, R. Jose, *Nanoscale Adv.* **2019**, *1*, 3807.

[212] S. Ghosh, S. Barg, S. M. Jeong, K. Ostrikov, *Adv. Energy Mater.* **2020**, *10*, 2001239.

[213] K. Keum, J. W. Kim, S. Y. Hong, J. G. Son, S. S. Lee, J. S. Ha, *Adv. Mater.* **2020**, *32*, 2002180.

[214] L. Miao, Z. Song, D. Zhu, L. Li, L. Gan, M. Liu, *Energy Fuels* **2021**, *35*, 8443.

[215] Q. Dou, H. S. Park, *Energy Environ. Mater.* **2020**, *3*, 286.

[216] X. Zhang, C. Jiang, J. Liang, W. Wu, *J. Mater. Chem. A* **2021**, *9*, 8099.

[217] Y. M. Abbas, A. B. Mansour, S. E. Ali, A. H. Ibrahim, *J. Magn. Magn. Mater.* **2019**, *482*, 66.

[218] W. Zhao, C. Guo, C. M. Li, *J. Mater. Chem. A* **2017**, *5*, 19195.

[219] B. Balakrishnan, S. K. Balasingam, K. S. Nallathambi, A. Ramadoss, M. Kundu, J. S. Bak, I. H. Cho, P. Kandasamy, Y. Jun, H.-J. Kim, *J. Ind. Eng. Chem.* **2019**, *71*, 191.

[220] D. T. Pham, J. P. Baboo, J. Song, S. Kim, J. Jo, V. Mathew, M. H. Alfaruqi, B. Sambandam, J. Kim, *Nanoscale* **2018**, *10*, 5938.

[221] C. Chen, Y. Yang, X. Tang, R. Qiu, S. Wang, G. Cao, M. Zhang, *Small* **2019**, *15*, 1804740.

[222] S. S. Karade, P. Dwivedi, S. Majumder, B. Pandit, B. R. Sankapal, *Sustainable Energy Fuels* **2017**, *1*, 1366.

[223] A. M. Zardkhoshoui, S. S. H. Davarani, A. A. Asgharinezhad, *Dalton Trans.* **2019**, *48*, 4274.

[224] X. Chen, T. Shi, K. Zhong, G. Wu, Y. Lu, *Chem. Eng. J.* **2020**, *379*, 122240.

[225] I. K. Durga, S. S. Rao, R. M. N. Kalla, J.-W. Ahn, H.-J. Kim, *J. Energy Storage* **2020**, *28*, 101216.

[226] X. Liu, L. Liu, W. Yan, Y. Wang, C. Huang, Z. Wang, *Energy Technol.* **2020**, *8*, 2000544.

[227] Z. Sun, F. Li, Z. Ma, Q. Wang, F. Qu, *J. Alloys Compd.* **2021**, *854*, 157114.

[228] M. Zhang, H. Liu, Y. Wang, T. Ma, *J. Colloid Interface Sci.* **2019**, *536*, 609.

[229] S.-x. Yan, S.-h. Luo, H. Liu, L. Yang, Q. Wang, Y.-h. Zhang, X. Liu, *Surf. Coat. Technol.* **2022**, *429*, 127980.

[230] Y. Yao, J. Wang, X. Ban, C. Chen, Q. Wang, K. Zhu, K. Ye, G. Wang, D. Cao, J. Yan, *EcoMat* **2023**, *5*, 12287.

[231] H. Sun, L. Zheng, Y. Xi, S. Zhai, Q. An, Z. Xiao, *Electrochim. Acta* **2023**, *466*, 143053.

[232] S. Hassanpoor, E. Tamri, *J. Alloys Compd.* **2023**, *932*, 167711.

[233] L. Shi, Z. Wang, N. Wu, X. Chen, G. Yang, W. Liu, *Int. J. Electrochem. Sci.* **2020**, *15*, 3204.

[234] Y. V. Lim, X. L. Li, H. Y. Yang, *Adv. Funct. Mater.* **2021**, *31*, 2006761.

[235] A. Ahmad, S. Shaheen, S. Majeed, M. Pervaiz, Z. Saeed, U. Younas, M. S. Javed, R. Luque, L. Gnanasekaran, *Fuel* **2023**, *340*, 127399.

[236] Z. Cao, H. Song, B. Cao, J. Ma, X. Chen, J. Zhou, Z. Ma, *J. Power Sources* **2017**, *364*, 208.

[237] X. Wang, Q. Xiang, B. Liu, L. Wang, T. Luo, D. Chen, G. Shen, *Sci. Rep.* **2013**, *3*, 2007.

[238] W. Deng, J. Chen, L. Yang, X. Liang, S. Yin, X. Deng, G. Zou, H. Hou, X. Ji, *Small* **2021**, *17*, 2101058.

[239] A. K. Haridas, J. Jeon, J. Heo, Y. Liu, R. Saroha, J. H. Joo, H.-J. Ahn, K.-K. Cho, J.-H. Ahn, *ACS Sustainable Chem. Eng.* **2019**, *7*, 6870.

[240] X. Luo, Y. Li, X. Cheng, *Ceram. Int.* **2023**, *49*, 27277.

[241] T. Li, H. Dong, Z. Shi, W. Liu, H. Yue, Y. Yin, X. Li, X. Wu, B. Li, S.-T. Yang, *ACS Appl. Nano Mater.* **2022**, *5*, 8835.

[242] Y.-X. Wang, J. Yang, S.-L. Chou, H. K. Liu, W.-x. Zhang, D. Zhao, S. X. Dou, *Nat. Commun.* **2015**, *6*, 8689.

[243] J. S. Cho, J.-S. Park, Y. C. Kang, *Nano Res.* **2017**, *10*, 897.

[244] D. Li, Y. Sun, S. Chen, J. Yao, Y. Zhang, Y. Xia, D. Yang, *ACS Appl. Mater. Interfaces* **2018**, *10*, 17175.

[245] F. Zhang, C. Wang, G. Huang, D. Yin, L. Wang, *J. Power Sources* **2016**, *328*, 56.

[246] L. Fei, Y. Jiang, Y. Xu, G. Chen, Y. Li, X. Xu, S. Deng, H. Luo, *J. Power Sources* **2014**, *265*, 1.

[247] Y. Du, S. Wu, M. Huang, X. Tian, *Chem. Eng. J.* **2017**, *326*, 257.

[248] Y. Yamaguchi, T. Takeuchi, H. Sakaebe, H. Kageyama, H. Senoh, T. Sakai, K. Tatsumi, *J. Electrochem. Soc.* **2010**, *157*, A630.

[249] H.-H. Fan, H.-H. Li, K.-C. Huang, C.-Y. Fan, X.-Y. Zhang, X.-L. Wu, J.-P. Zhang, *ACS Appl. Mater. Interfaces* **2017**, *9*, 10708.

[250] W. Chen, S. Qi, L. Guan, C. Liu, S. Cui, C. Shen, L. Mi, *J. Mater. Chem. A* **2017**, *5*, 5332.

[251] Y. Liu, X.-Y. Yu, Y. Fang, X. Zhu, J. Bao, X. Zhou, X. W. D. Lou, *Joule* **2018**, *2*, 725.

[252] K. Zhang, M. Park, L. Zhou, G. H. Lee, J. Shin, Z. Hu, S. L. Chou, J. Chen, Y. M. Kang, *Angew. Chem., Int. Ed.* **2016**, *55*, 12822.

[253] Y. Zhu, L. Suo, T. Gao, X. Fan, F. Han, C. Wang, *Electrochem. Commun.* **2015**, *54*, 18.

[254] A. Kitajou, J. Yamaguchi, S. Hara, S. Okada, *J. Power Sources* **2014**, *247*, 391.

[255] K. Chen, G. Li, Y. Wang, W. Chen, L. Mi, *Green Energy Environ.* **2020**, *5*, 50.

[256] H. Zhang, H. Ming, W. Zhang, G. Cao, Y. Yang, *ACS Appl. Mater. Interfaces* **2017**, *9*, 23766.

[257] L. Fei, Q. Lin, B. Yuan, G. Chen, P. Xie, Y. Li, Y. Xu, S. Deng, S. Smirnov, H. Luo, *ACS Appl. Mater. Interfaces* **2013**, *5*, 5330.

[258] M. Walter, T. Zünd, M. V. Kovalenko, *Nanoscale* **2015**, *7*, 9158.

[259] P. Zhao, H. Cui, J. Luan, Z. Guo, Y. Zhou, H. Xue, *Mater. Lett.* **2017**, *186*, 62.

[260] S.-P. Guo, J.-C. Li, Z. Ma, Y. Chi, H.-G. Xue, *J. Mater. Sci.* **2017**, *52*, 2345.

[261] J. Mao, T. Zhou, Y. Zheng, H. Gao, H. kun Liu, Z. Guo, *J. Mater. Chem. A* **2018**, *6*, 3284.

[262] C. Xing, D. Zhang, K. Cao, S. Zhao, X. Wang, H. Qin, J. Liu, Y. Jiang, L. Meng, *J. Mater. Chem. A* **2015**, *3*, 8742.

[263] L. Fei, B. P. Williams, S. H. Yoo, J. M. Carlin, Y. L. Joo, *Chem. Commun.* **2016**, *52*, 1501.

[264] T. Evans, D. M. Piper, S. C. Kim, S. S. Han, V. Bhat, K. H. Oh, S. H. Lee, *Adv. Mater.* **2014**, *26*, 7386.

[265] S. S. Zhang, *J. Mater. Chem. A* **2015**, *3*, 7689.

[266] Y. He, M. Luo, C. Dong, X. Ding, C. Yin, A. Nie, Y. Chen, Y. Qian, L. Xu, *J. Mater. Chem. A* **2019**, *7*, 3933.

[267] P. Ramakrishnan, S.-H. Baek, Y. Park, J. H. Kim, *Carbon* **2017**, *115*, 249.

[268] F. Cao, G. Pan, J. Chen, Y. Zhang, X. Xia, *J. Power Sources* **2016**, *303*, 35.

[269] Q.-T. Xu, J.-C. Li, H.-G. Xue, S.-P. Guo, *J. Power Sources* **2018**, *396*, 675.

[270] D. T. Tran, S. S. Zhang, *J. Mater. Chem. A* **2015**, *3*, 12240.

[271] Y. Yao, J. Zheng, Z. Gong, Z. Ding, J. Zhang, W. Yu, D. M. Bengono, H. Li, B. Zhang, H. Tong, *J. Alloys Compd.* **2019**, *790*, 288.

[272] J. Lin, Z. Peng, W. Yang, Z. Liu, X. Liu, R. Sun, Z. Qin, H. Fan, Y. Zhang, *Electrochim. Acta* **2021**, *392*, 139071.

[273] S. Deng, S. Xiong, X. Wang, S. Wang, Z. Zhao, L. Hou, Y. Jiang, F. Gao, *Electrochim. Acta* **2023**, *437*, 141517.

[274] R. Zeng, J. Zhang, H.-B. Guan, S.-G. Wang, T. Qin, Y.-L. Hou, D.-L. Zhao, *J. Alloys Compd.* **2022**, *928*, 167244.

[275] L. Fu, W. Xiong, Q. Liu, S. Wan, C. Kang, G. Li, J. Chu, Y. Chen, S. Yuan, *J. Alloys Compd.* **2021**, *869*, 159348.

[276] Q. Li, Y. Liu, S. Wei, L. Xu, X. Wu, W. Wu, *J. Electroanal. Chem.* **2021**, *903*, 115848.

[277] A. K. Haridas, H. Kim, C.-H. Choi, H.-J. Ahn, J.-H. Ahn, *Appl. Surf. Sci.* **2021**, *554*, 149587.

[278] P. Song, J. Li, Y. Zhang, F. Tang, C. Wang, D. Su, T. Wang, *J. Alloys Compd.* **2023**, *950*, 169905.

[279] L. Zhang, F. Peng, M. Zhang, D. Li, Q. Pan, G. Yang, F. Zheng, Y. Huang, H. Wang, Q. Li, *Appl. Surf. Sci.* **2022**, *606*, 154864.

[280] H. Zhou, F. Ling, H. Zhou, J.-c. Wu, X. Li, D. Hou, J. Ge, T. Xu, H. Gao, *J. Alloys Compd.* **2023**, *941*, 168886.

[281] Z. Wu, W. Zhang, Y. Xia, H. Huang, Y. Gan, X. He, X. Xia, J. Zhang, *EcoMat* **2023**, *5*, 12327.

[282] R. Yang, C. Wang, Y. Li, Z. Chen, M. Wei, *J. Electroanal. Chem.* **2022**, *918*, 116467.

[283] Z. Li, Y. Zhang, X. Li, F. Gu, L. Zhang, H. Liu, Q. Xia, Q. Li, W. Ye, C. Ge, *J. Am. Chem. Soc.* **2021**, *143*, 12800.

[284] X. Zhao, D.-A. Zhang, C. Sun, J. Liu, T. Zhao, M. Wang, Y. Song, H. Xu, Q. Wang, *J. Electroanal. Chem.* **2022**, *922*, 116724.

Ahmad Farhan got his M.Phil in chemistry from the University of Agriculture, Faisalabad, Pakistan, in 2022. Author of 18 JCR publications with a collective impact factor exceeding 70. Currently, he serves as a visiting lecturer in chemistry at the University of Agriculture Faisalabad (sub-campus Burewala). His research pursuits are directed towards the synthesis of advanced carbon-based materials, focusing on their applications in photocatalytic water remediation, as well as energy production and storage.

Wajeeha Qayyum holds an M.Phil in chemistry from the University of Agriculture, Faisalabad, where her research focused on carbon quantum dots, metal ferrites, and graphene oxide-based materials for water treatment. With a total of five publications to her credit, she demonstrates a strong dedication to academic inquiry and innovation in her field. Her interests have expanded to include electrocatalytic applications aimed at advancing the production of greener energy sources, reflecting her commitment to sustainable technology development.

Urooj Fatima holds an M.Phil in chemistry from the University of Agriculture, Faisalabad. During her academic pursuits, she does her research into the intricate world of wastewater treatment, focusing extensively on the impact of dyes on water quality. Through rigorous investigation and experimentation, she has aimed to contribute meaningfully to the development of sustainable solutions for wastewater management. Beyond academia, she is currently engaged as a Monitoring Officer in the Education Department, where she continues to apply her expertise in research methodologies to monitor and assess educational initiatives. This role allows her to leverage her analytical skills to ensure the effective implementation of educational programs, ultimately striving to enhance learning outcomes for students. She remains deeply committed to the pursuit of knowledge and innovation, driven by a desire to make a positive impact on society.

Shahid Nawaz is currently a Ph.D. scholar at the State Research Institute Physical and Technological Sciences Center (FTMC), Vilnius, Lithuania. He received his master's degree from the University of Lahore, Pakistan. With a notable publication record that includes 23 papers, he had earned over 604 citations and achieved an h-index of 9. His research focuses on catalysts for renewable energy, photocatalytic properties of nanomaterial for wastewater, recent advancements in environmental remediation, and synthesis and applications of heterogeneous catalysts.

Aldona Balčiūnaitė is a senior research associate at the Center for Physical Sciences and Technology. In 2017, she defended her doctoral dissertation on "New materials for alkaline fuel cells: Synthesis, characterization, and properties". Her main research areas include fuel cells, catalysts, electroless metal deposition, and electrochemical methods of analysis. Her research area is related to promising, worldwide intensive research into the properties of materials used in fuel cells. It is focused on the search for new efficient materials that can be applied in direct alkaline fuel cells to enhance the performance of existing or new fuel cells.
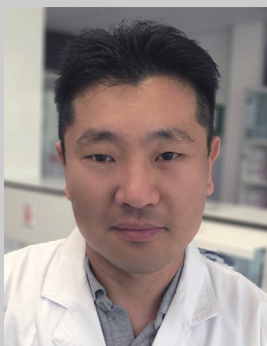
Tak Kim is currently leading a small but dynamic research group under the School of Environment and Science at Griffith University. He has been working toward the development of nanomaterials for biomedical, environmental, and energy applications since the completion of his Ph.D. in 2016. He also has been working with industry research collaborators and government agencies to develop sustainable recycling technologies for end-of-life tires and out-of-date chemical powder extinguishers, aiming to foster a circular economy.

Varsha Srivastava is currently working as an associate professor (tenure track) in the Research Unit of Sustainable Chemistry at Oulu University, Finland. She received her Ph.D. degree in 2009 from IIT-BHU, India. She has published over 126 articles in various peer-reviewed international journals. Her research interests include biomass valorization, biomass refining, bio-sorbents, biodiesel synthesis, heterogeneous catalysts, inorganic/organic hybrid functional materials, photocatalysis, wastewater treatment, and resource recovery from solid and liquid waste streams.

John Vakros serves now as a researcher in the Department of Chemical Engineering at the University of Patras, Greece. He holds a diploma in chemistry (1992), and a Ph.D. (1997) from the University of Patras. His research activities focus on heterogeneous catalytic processes, acid-base behavior of solids, evaluation of biochars, and, over the last five years, in circular economy. Emphasis is given to catalytic measurements for environmental applications, determination of interactions of reactants with catalytic surface groups, and tuning the physicochemical properties of supported catalysts. He is the author of more than 85 articles in scientific journals.

Zacharias Frontistis is an associate professor specializing in water process engineering at the Department of Chemical Engineering, University of Western Macedonia. His research focuses on catalysis for environmental and energy applications, the development of new physicochemical processes for water treatment (AOPs), combining physicochemical and biological processes for advanced wastewater treatment and simulating these processes. He has published over 150 articles in international journals (h-index = 46, 6000 citations). He is on the editorial board of six international journals and has been a guest editor for 13 special issues. He has participated in more than 17 European and national projects.

Grzegorz Boczkaj is an associate professor at Gdansk University of Technology (GUT), Poland. He obtained a Ph.D. with honors in chemical technology (chemical engineering) at GUT (2012) and a habilitation in the same discipline (2017). He is the leader scientist of a research group working on new developments in the field of environmental science, separation techniques, chemical engineering as well as analytical chemistry. He was a principal investigator of several research projects (in total above 2 mln USD). He has published over 200 journal articles, book chapters, and technical reports (h-index: 48, > 8800 citations). Scientific profiles: Google Scholar; SCOPUS.